Applied Energy 309 (2022) 118453

Contents lists available at ScienceDirect

Applied Energy

journal homepage: www.elsevier.com/locate/apenergy

Optimal operation of a multi-generation district energy hub based on electrical, heating, and cooling demands and hydrogen production

Amir Ebrahimi-Moghadam *, Mahmood Farzaneh-Gord *

Mechanical Engineering Department, Faculty of Engineering, Ferdowsi University of Mashhad, Mashhad, Iran

HIGHLIGHTS

- A Multi-generation energy hub is proposed based on power, heat, cold, and hydrogen.
- Strong eco-exergy and enviro-exergy analyses are presented.
- Optimal operating conditions are sought using a robust multi-objective optimization.
- Optimal outputs: 21.42 MW power, 26.81 MW heat, 8.89 MW cold, and 11.96 kg/h hydrogen.
- The payback period is approximately 5 years at the optimal conditions.

GRAPHICAL ABSTRACT

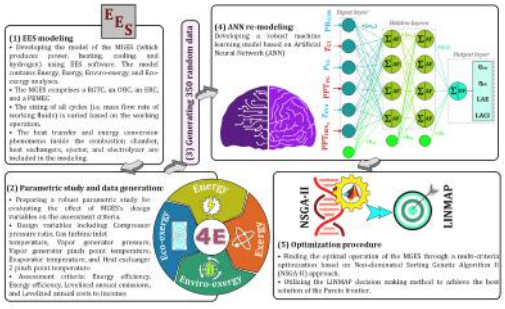

ARTICLE INFO

Keywords:
Multi-generation district energy hub
Power to gas (P2G)
Hydrogen production
Eco-exergy analysis
Enviro-exergy analysis
Multi-criteria optimization

ABSTRACT

In this study, a new configuration of a multi-generation energy system is proposed based on waste heat recovery from a regenerative gas turbine cycle (as the driver cycle) for running a district heating heat exchanger, a Rankine cycle, an ejector refrigeration cycle, and a proton exchange membrane electrolyzer cycle. In the first phase of the study, a thorough parametric model of the system is developed in EES software based on the eco-exergy and enviro-exergy analyses. The second phase is focused on the optimal operation of the system utilizing a robust multi-criteria optimization in Matlab software. Results of the parametric study showed that: (i) the share of fuel, capital, and environmental penalty costs rates in the system's total cost rate are respectively 46.95%, 29.38%, and 23.67%, at the optimal conditions. (ii) although the design variables of the bottoming cycles are not effective on the amount of pollutants, they have a significant effect on the enviro-exergy assessment criterion. The optimal system productions are included 21.42 MW of power, 26.81 MW of heat, 8.89 MW of cold, and 11.96 kg/h of hydrogen. The energy and exergy efficiencies are found to be 89.75% 35.21%, respectively. In such conditions, the payback period is approximately 5 years, demonstrating the economic feasibility of the proposal. Recovering the waste heat of conventional cycles to develop an energy production hub with minimal energy loss is one of the most important challenges in the energy matrix and relying on the results of the present study, it can be concluded that the proposed system has done this task well.

* Corresponding authors.
E-mail addresses: amir_ebrahimi_051@yahoo.com (A. Ebrahimi-Moghadam), m.farzanehgord@um.ac.ir (M. Farzaneh-Gord).

https://doi.org/10.1016/j.apenergy.2021.118453
Received 2 June 2021; Received in revised form 25 July 2021; Accepted 25 December 2021

Nomenclature

Parameters and variables

A	area [m^2]
AS	annual savings [$]
c	cost per exergy unit [$/GJ]
$\dot{C}$	cost rate [$/yr]
COP	coefficient of performance [-]
CRC	capital recovery coefficient [-]
D	thickness of membrane [μm]
E	energy [kJ]
ex	specific exergy [kJ/kg]
$\dot{E}x$	exergy rate [kW]
F	Faraday constant [C/mol]
FC	fixed costs [$]
g	gravitational acceleration [m/s^2]
G	Gibbs free energy [J/kmol]
h	specific enthalpy [kJ/kg], heat transfer coefficient [kW/m^2 K]
i_{eff}	effective interest rate [%]
IF	inflation factor [-]
J	current density [A/m^2]
k	conductivity [kW/m K]
LACI	levelized annual costs to incomes [-]
LAE	levelized annual emissions [kg/GJ]
LHV	lower heating value [kJ/kg]
LMTD	logarithmic mean temperature difference [K]
m	pollutant emission per unit burned fuel [$g_{pollutant}/kg_{fuel}$]
$\dot{m}$	mass flow rate [kg/s]
n	number of moles [kmol]
N	expected life span [yr]
$\dot{N}$	molar flow rate [kmol/s]
NPV	net present value [$]
Nu	Nusselt number [-]
P	pressure [bar]
PEC	purchase equipment cost [$]
PPT	pinch point temperature [K]
Pr	Prandtl number [-]
PR	pressure ratio [-]
$\dot{Q}$	heat transfer rate [kW]
r	rate of inflation [%]
R	gas constant [kJ/kmol K]
$\overline{R}$	universal gas constant [kJ/kmol K]
RDF	real discount factor [-]
Re	Reynolds number [-]
s	specific entropy [kJ/kg K]
t_{year}	operating hours during a year [h/y]
T	temperature [K]
u	velocity [m/s]
U	overall heat transfer coefficient [kW/m^2 K]
V	voltage [V]
$\dot{W}$	power [kW]
z	height [m]
$\dot{Z}$	equipment cost rate [$/yr]

Greek symbols

η	efficiency [%]
Φ	maintenance factor [-]
$\varnothing$	combustion equivalence ratio [-]
λ	membrane surface water [1/Ω]
$\overline{\lambda}$	molar fuel–air ratio [-]
μ	viscosity [$N.s/m^2$]
$\mathscr{T}$	combustion residence time [s]
$\dot{\Psi}$	exergy destruction rate [kW]
σ	ionic conductivity [-]

Abbreviations and subscripts

0	environmental conditions
4E	energy, exergy, economic, and environmental
a	anode
act	activation
ANN	artificial neural network
AP	air pre-heater
c	cathode
ch	chemical
CC	combustion chamber
CCHP	combined cooling, heating, and power
CCP	combined cooling and power
CGES	co-generation energy system
CHP	combined heating and power
CO	carbone monoxide
CO_2	carbon dioxide
COM	compressor
CON	condenser
D	diffuser of ejector
D	destruction (exergy)
en	energy
env	environmental
ex	exergy
EES	engineering equation solver
EJ	ejector
ERC	ejector refrigeration cycle
EV	expansion valve
EVA	evaporator
f	fuel
GA	genetic algorithm
GT	gas turbine
GTC	gas turbine cycle
H_2	hydrogen
HEX	heat exchanger
H_2O	water
in	inlet
k	equipment k
LINMAP	linear programming technique for multidimensional analysis of preference
M	mixing chamber of ejector
MCO	multi-criteria optimization
MF	mixed flow (in ejector)
MGES	multi-generation energy system
net	net value
N	nozzle of ejector
N_2	nitrogen
NG	natural gas
NOx	nitrogen oxide
NSGA −II	non-dominated sorting GA II
ohm	ohmic
out	outlet
O_2	oxygen
O&M	opterating and maintenance
ORC	organic Rankine cycle
ph	physical (in exergy)
P2G	power to gas
PEME	proton exchange membrane electrolyzer
PEMEC	PEME cycle
PF	primary flow (in ejector)
ph	physical (in exergy)
PU	pump
PZ	primary zone of the CC
ref	reference

RC	Rankine cycle	ST	steam turbine
RGTC	regenerative gas turbine cycle	TGES	tri-generation energy system
s	isentropic	VG	vapor generator
SEP	separator	WHR	waste heat recovery
SF	secondary flow (in ejector)		

1. Introduction

As two essential needs of human life, energy and water are vital issues of any governments all around the world [1,2]. Although water covers 70% of the earth's surface, about 15% of the world's population deprived of access to drinking water [3]. On the other hand, factors such as increasing modernization and industrialization of cities and environmental pollution caused by urban sprawl have led to increased energy consumption in the last decades [4]. Hence, these factors have led to two issues becoming the most prominent issues in the field of energy: (1) the production and use of sustainable energy carriers, (2) the use of new methods to minimize energy losses.

Hydrogen is one solution for the first mentioned issue. Among most chemical fuels, hydrogen has the highest energy content by weight (for example, 3 times higher than gasoline) and it is also considered a clean fuel. For the second issue, developing hybrid energy systems based on the WHR (waste heat recovery) of available systems has attracted much attention [5]. Using these systems results in several benefits including: the ability of producing different kinds of energies in a unique unit, higher efficiency by recovering the wasted heat of a basic system, and lower pollutions and costs per system productions compared to the basic system [6].

Based on the system productions, the hybrid energy systems could be categorized into three main groups including co-, tri-, and multi-generation energy systems (CGES, TGES, and MGES). Based on the design requirements, the system production could be power (electricity), heat, cold, hydrogen, or freshwater. Furthermore, CCP (combined cooling and power) [7], CHP (combined heating and power) [8], and CCHP (combined cooling, heating and power) [9] systems are another classification of these systems.

The gas turbine cycle (GTC) is one of the widely used conventional power generation systems in the world. The flue gas of this cycle, which is discharged into the atmosphere in the basic system mode, has a high temperature and could be used as heat source of some other cycles to develop a new hybrid energy system. Reviewing the available previous published works in this research field, the Rankine cycle (RC), organic RC (ORC), Kalina cycle (KC), ejector refrigeration cycle (ERC), absorption refrigeration cycle (ARC), proton exchange membrane electrolyzer cycle (PEMEC) are the most widely used cycles as bottoming cycles for recovering heating potential of the GTC [10–12]. In the category of MGES, Zoghi et al. [13] developed eco-exergy and environmental models for evaluating a MGES based on the WHR from a solar-assisted biogas-fired regenerative GTC (RGTC). Their system had the ability to produce electricity, heat, cold, and hydrogen and the bottoming cycles were included a RC, an ARC, and a PEMEC. Their results showed that although increasing the number of mirrors in the solar section reduces fuel consumption and pollutant emissions, it hurts the energetic and economic criteria of the system. Park et al. [14] used Aspen-Hysys commercial software for developing thermodynamics model of a MGES (CCHP + H_2) hybrid cycle. Their proposed system generated 1.73 MW_e power, results in maximum energetic efficiency of 87.43%. In another work, Safder et al. [15] investigated a new layout of MGESs from 4E[1] standpoints. The system was constructed from five sub-cycles (GTC, RC, KC, ERC, and water desalination cycle). In their proposal, the maximum amount of system productions were 28.73 MW of power, 3.43 MW of cooling, and 13.64 kg/s of freshwater. Nazari and Porkhial [16] proposed a MGES (CCHP + freshwater) based on the retrieval of the heating potential of flue gases from solar-assisted biogas-fired RGTC (as mover cycle) for setting up four sub-cycles including a RC, an ORC, an ARC, and a water desalination unit. They achieved exergetic efficiency of 20.5% and total cost rate of 69.2 $/h at optimum conditions.

In some other studies, the effort was focused on TGESs. Recently, Azariyan et al. [17] designed a system for producing cold and hydrogen using by the generated power of a geothermal KC. The sub-cycles were comprised of ARC (to produce cold) and PEMEC (to produce hydrogen). Defining a base working condition, they found that energetic efficiency, exergetic efficiency, and total productions cost rate of 22.28%, 21.37%, and 29.29 $/GJ, respectively. With the use of HOMER software, Peláez-Peláez et al. [18] accomplished thermo-economic assessment of a hydrogen-based CHP plant. The energy cost of their system was 0.84 $/kWh and they concluded that although their proposal is technically feasible, it is not economic-friendly. Ebrahimi-Moghadam et al. [19] conducted a research work based on the eco-exergy and enviro-exergy analyses of a novel TGES for district energy systems. They also presented the optimal operating conditions of the system containing 1.03 MW of power, 1.64 MW of heat, and 304.9 kW of cold. Di Marcoberardino et al. [20] used the thermodynamics and economics principles to evaluate a micro-scale CHP system which was containing two low-temperature and high-temperature PEM fuel cells integrated with a steam reformer. Their report showed that the maximum total energetic efficiency of the system is around 88% for residential applications in Italy (as a case study). In another published work, Lümmen et al. [21] combined an ORC with a PEMEC and introduced a TGES which produces power, heat, and hydrogen. Depending on the operating condition, their system could produce 186–364 ton/yr hydrogen.

In the CGES category, Alirahmi et al. [22] designed a new green combined cycle based on the combination of solar RGTC and PEMEC integrated with a compressed air energy storage. They evaluated the feasibility of constructing their proposal in Los Angeles (as a case study) and reached an investment recovery time of 4.6 years. Ahmadi et al. [23] introduced a CGES for generating electricity and producing hydrogen simultaneously. The system was made by combining gas and air cycles (for electricity) with a natural gas (NG) reformer (for hydrogen). They utilized 4E models to assess their proposal and found that the investment recovery time is reduced from 4.72 years to 2.92 years by using the proposed hybrid system instead of the base system. Li et al. [24] sought out the optimal working conditions of an electricity-hydrogen CGES comprises an ORC and a PEMEC. They considered net generated power and total cost rate as two optimization functions and found their optimum value to be 1571.1 kW and 10.51 $/h, respectively. In another work, Datas et al. [25] proposed a concept of a residential energy system for converting power to heat and vice versa. Relying on a thermo-economic study, they reached to payback period of lower than 15 years. Moharamian et al. [26] recovered the exhaust gases of a modified GTC to run a RC, and then used the generated power of the RC to run a PEMEC. Applying 4E parametric analysis, they studied the effects of two important design parameters of the GTC (PR_{COM} and T_{GT}) on the system performance. By injecting the produced hydrogen into the combustion chamber, their results showed 46% and 27% reduction in fuel consumption and CO_2 emission, respectively.

Supplying different kinds of required energy with the lowest environmental impacts and using green energy carriers (such as hydrogen) are among serious challenging issues in the world. In addition,

[1] 4E: Energy, Exergy, Economic, and Environmental

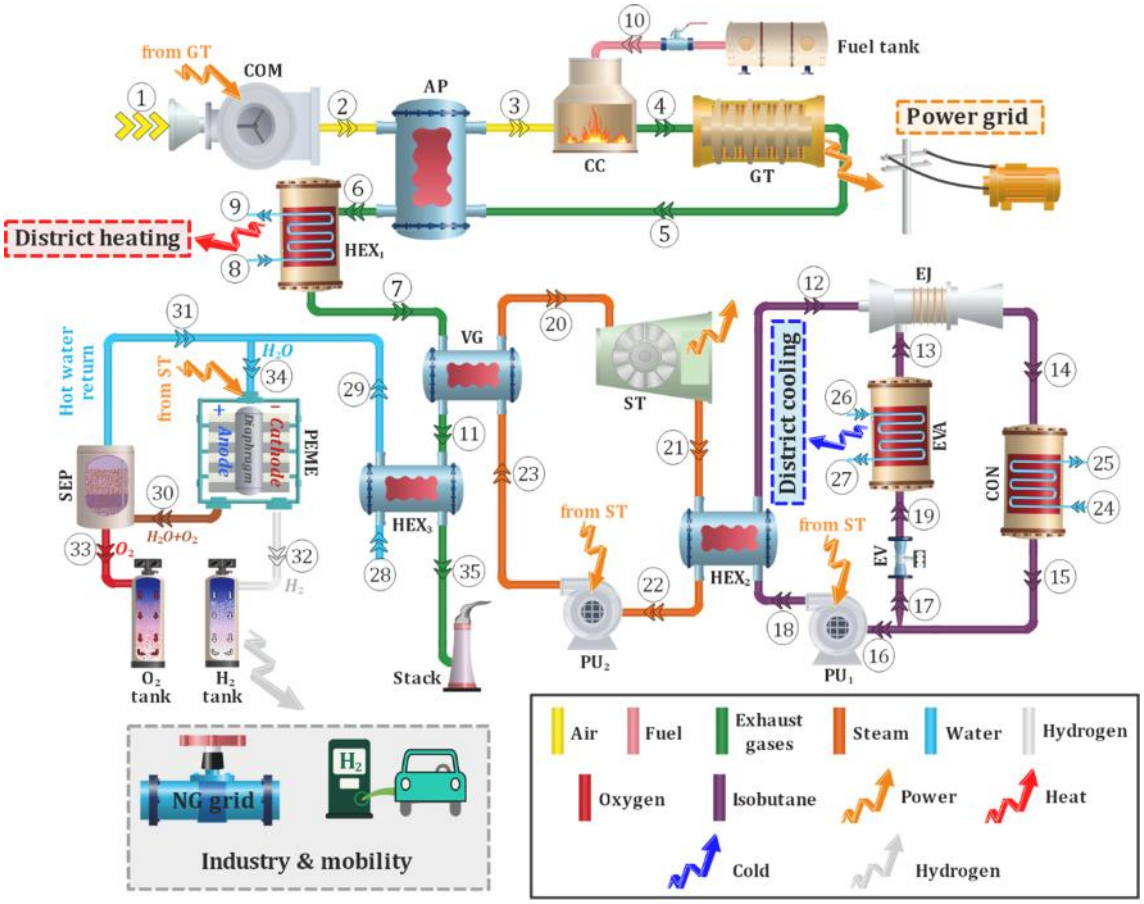

Fig. 1. The outline of the introduced MGES; COM: compressor, AP: air pre-heater, CC: combustion chamber, GT: gas turbine, HEX: heat exchanger, VG: vapor generator, ST: steam turbine, PU: pump, EJ: ejector, EVA: evaporator, CON: condenser, EV: expansion valve, PEME: proton exchange membrane electrolyzer, SEP: separator.

proposing efficient and economic-friendly ways to achieve this goal are the other important aspects that must be addressed by science and technology. Recovering the wasted heating load of available conventional power generation cycles for running some new sub-cycles (as MGES) is one of the major strategies in this field of study. In the past studies, different layouts of MGESs based on the GTC as the mover cycle are introduced. But to the best of the authors' knowledge, combination of the RGTC, RC, ERC, and PEMEC could be considered as a new MGES configuration. Furthermore, the literature is still demanding strong eco-exergy and enviro-exergy evaluation of MGESs, as the analysis of such systems is mostly limited to sustainability exponents without attention to the impact of energy conversion on the economy and environment. Accordingly, in this study, the efforts are firstly focused on the development of a hybrid MGES (acts as a hub based on the district energy conditions) in which the maximum possible utilization of the waste heat of the RGTC is used in such a way that the system to not only be economically viable, but also a sustainable and environmentally-friendly system. After designing the novel proposed MGES, the answer to some important questions is sought in this study: (1) What are the most effective variables in the design of this system? How and to what extent do these variables affect the system efficiency and enviro-eco indicators? (2) What are the optimal operating conditions of the proposed MGES? What are the optimum values of the system efficiency and enviro-eco indicators?

In a nutshell, to bridge the mentioned gap in the literature and achieve the answer to the mentioned questions, the following items are the contribution of this study and the considered novelties:

- ***Novelty in system layout:*** To the best of the authors' knowledge, introducing a new MGES based on the WHR from RGTC for running RC, ERC, and PEMEC (as bottoming sub-cycles) is a new layout which has not been investigated yet. The system acts as a district energy hub through simultaneous production of power, heat, cold, and hydrogen.
- ***Novelties in methodology:*** Unlike most previous studies, which considered the system equipment as a black-box for energy modeling, in the present study, the heat transfer and energy conversion phenomena inside the combustion chamber, heat exchangers, ejector, and electrolyzer have been modeled with real assumptions. Furthermore, a potent thermodynamic model with real assumptions and variable system sizing depending on the operating conditions is developed. This means that, unlike majority of previous studies in the field, the mass flow rates of the working fluids in all of the sub-cycles are considered as the problem outputs and are not fixed. Developing a detailed and powerful framework for evaluating the system from eco-exergy and enviro-exergy standpoints is another aspect of the novelties in the methodology of this paper. These analyses have advantages in the evaluation of MGESs, compared to the conventional analyses.
- ***Novelty in optimization:*** A multi-criteria optimization (MCO) is done by combining artificial neural network (ANN) and non-dominated sorting GA II (NSGA-II) methods. Presenting the optimal operating conditions of the system based on this thorough approach with four objective functions is a novel aspect in the available literature.

To achieve the above-mentioned goals, the rest of the study is

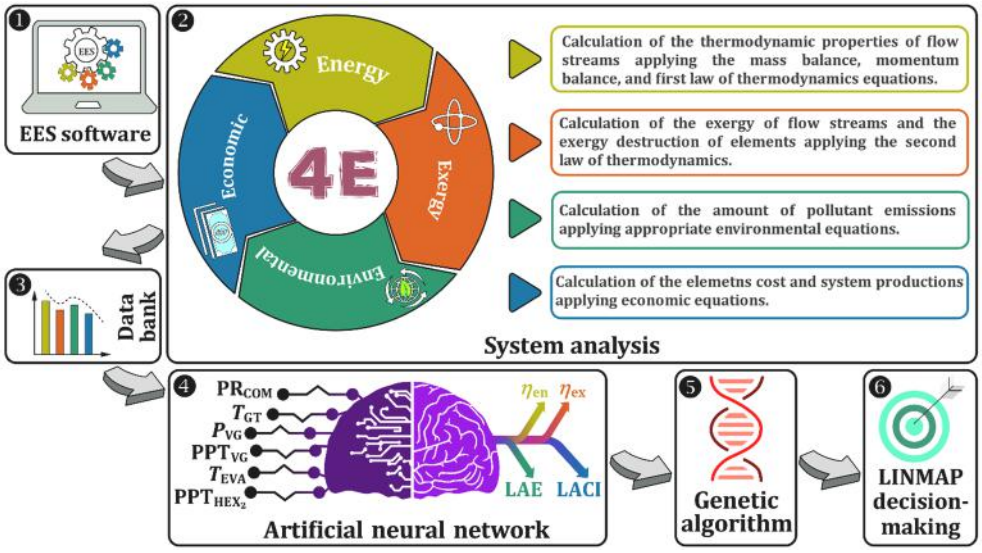

Fig. 2. An illustrative sketch for different steps of the modeling and optimization procedures.

Table 1
Final form of the main equations for the energy and exergy models.

Cycle	Equipment name	Mass balance	Energy model	Exergy model
Regenerative gas turbine cycle	Compressor	$\dot{m}_1 = \dot{m}_2 = \dot{m}_a$	$\dot{W}_{COM} = \dot{m}_1(h_2 - h_1)$,$\eta_{COM,s} = \frac{h_{2,s} - h_1}{h_2 - h_1}$	$\dot{\Psi}_{COM} = \dot{W}_{COM} - \left(\dot{E}x_2 - \dot{E}x_1\right)$
	Air pre-heater	$\dot{m}_2 = \dot{m}_3; \dot{m}_5 = \dot{m}_6$	$\dot{Q}_{AP} = \dot{m}_2(h_3 - h_2) = \dot{m}_5(h_5 - h_6)$	$\dot{\Psi}_{AP} = \left(\dot{E}x_5 - \dot{E}x_6\right) - \left(\dot{E}x_3 - \dot{E}x_2\right)$
	Combustion chamber	$\dot{m}_3 + \dot{m}_{10} = \dot{m}_4 = \dot{m}_g \dot{m}_{10} = \dot{m}_f$	$\dot{m}_3 h_3 + \dot{m}_{10} \times LHV_f = \dot{m}_4 h_4 + (1 - \eta_{CC})\dot{m}_{10} \times LHV_f$	$\dot{\Psi}_{CC} = \left(\dot{E}x_3 + \dot{E}x_{10}\right) - \dot{E}x_4 - \left[\dot{Q}_{CC}(1 - \frac{T_0}{T_{CC}})\right]$
	Gas turbine	$\dot{m}_4 = \dot{m}_5$	$\dot{W}_{GT} = \dot{m}_5(h_4 - h_5)$,$\eta_{GT,s} = \frac{h_4 - h_5}{h_4 - h_{5,s}}$	$\dot{\Psi}_{GT} = \left(\dot{E}x_4 - \dot{E}x_5\right) - \dot{W}_{GT}$
Rankine cycle	Vapor generator	$\dot{m}_7 = \dot{m}_{11}; \dot{m}_{23} = \dot{m}_{20} = \dot{m}_{RC}$	$\dot{Q}_{VG} = \dot{m}_{11}(h_7 - h_{11}) = \dot{m}_{20}(h_{20} - h_{23})$	$\dot{\Psi}_{VG} = \left(\dot{E}x_7 - \dot{E}x_{11}\right) - \left(\dot{E}x_{20} - \dot{E}x_{23}\right)$
	Steam turbine	$\dot{m}_{20} = \dot{m}_{21}$	$\dot{W}_{ST} = \dot{m}_{21}(h_{20} - h_{21})$,$\eta_{ST,s} = \frac{h_{20} - h_{21}}{h_{20} - h_{21,s}}$	$\dot{\Psi}_{ST} = \left(\dot{E}x_{20} - \dot{E}x_{21}\right) - \dot{W}_{ST}$
	Heat exchanger 2	$\dot{m}_{21} = \dot{m}_{22}; \dot{m}_{18} = \dot{m}_{12}$	$\dot{Q}_{HEX_2} = \dot{m}_{21}(h_{21} - h_{22}) = \dot{m}_{18}(h_{12} - h_{18})$	$\dot{\Psi}_{HEX_2} = \left(\dot{E}x_{21} - \dot{E}x_{22}\right) - \left(\dot{E}x_{12} - \dot{E}x_{18}\right)$
	Pump 2	$\dot{m}_{22} = \dot{m}_{23}$	$\dot{W}_{PU_2} = \dot{m}_{22}(h_{23} - h_{22})$,$\eta_{PU_2,s} = \frac{h_{23,s} - h_{22}}{h_{23} - h_{22}}$	$\dot{\Psi}_{PU_2} = \dot{W}_{PU_2} - \left(\dot{E}x_{23} - \dot{E}x_{22}\right)$
Ejector refrigeration cycle	Ejector	$\dot{m}_{12} + \dot{m}_{13} = \dot{m}_{14} = \dot{m}_{ERC}\dot{m}_{12} = \dot{m}_{PF}$; $\dot{m}_{13} = \dot{m}_{SF}$	Refer to Table 2	$\dot{\Psi}_{EJ} = \left(\dot{E}x_{12} + \dot{E}x_{13}\right) - \dot{E}x_{14}$
	Evaporator	$\dot{m}_{19} = \dot{m}_{13}; \dot{m}_{26} = \dot{m}_{27}$	$\dot{Q}_{EVA} = \dot{m}_{13}(h_{13} - h_{19}) = \dot{m}_{26}(h_{26} - h_{27})$	$\dot{\Psi}_{EVA} = \left(\dot{E}x_{19} - \dot{E}x_{13}\right) - \left(\dot{E}x_{27} - \dot{E}x_{26}\right)$
	Condenser	$\dot{m}_{14} = \dot{m}_{15}; \dot{m}_{24} = \dot{m}_{25}$	$\dot{Q}_{CON} = \dot{m}_{14}(h_{14} - h_{15}) = \dot{m}_{24}(h_{25} - h_{24})$	$\dot{\Psi}_{CON} = \left(\dot{E}x_{14} - \dot{E}x_{15}\right) - \left(\dot{E}x_{25} - \dot{E}x_{24}\right)$
	Expansion valve	$\dot{m}_{17} = \dot{m}_{19}$	$h_{19} = h_{17}$	$\dot{\Psi}_{EV} = \dot{E}x_{17} - \dot{E}x_{19}$
	Pump 1	$\dot{m}_{16} = \dot{m}_{18}$	$\dot{W}_{PU_1} = \dot{m}_{16}(h_{18} - h_{16})$,$\eta_{PU_1,s} = \frac{h_{18,s} - h_{16}}{h_{18} - h_{16}}$	$\dot{\Psi}_{PU_1} = \dot{W}_{PU_1} - \left(\dot{E}x_{18} - \dot{E}x_{16}\right)$
PEM elctrolyzer cycle	Heat exchanger 3	$\dot{m}_{11} = \dot{m}_{35} = \dot{m}_g \dot{m}_{28} = \dot{m}_{29} = \dot{m}_{PEMEC}$	$\dot{Q}_{HEX_3} = \dot{m}_{35}(h_{11} - h_{35}) = \dot{m}_{28}(h_{29} - h_{28})$	$\dot{\Psi}_{HEX_3} = \left(\dot{E}x_{11} - \dot{E}x_{35}\right) - \left(\dot{E}x_{29} - \dot{E}x_{28}\right)$
	PEM elctolyzer	$\dot{m}_{34} = \dot{m}_{30} + \dot{m}_{32}\dot{m}_{32} = \dot{m}_{H_2}; \dot{m}_{30} = \dot{m}_{H_2O+O_2}$	Refer to Table 3	$\dot{\Psi}_{PEME} = \left(\dot{E}x_{34} + \dot{W}_{PEME}\right) - \left(\dot{E}x_{30} + \dot{E}x_{32}\right)$
	Separator	$\dot{m}_{30} = \dot{m}_{31} + \dot{m}_{33}\dot{m}_{33} = \dot{m}_{O_2}$	$\dot{m}_{30}h_{30} = \dot{m}_{31}h_{31} + \dot{m}_{33}h_{33}$	$\dot{\Psi}_{SEP} = \dot{E}x_{30} - \left(\dot{E}x_{31} + \dot{E}x_{33}\right)$

organized as four main sections including:

i) Section 2 begins with introducing the problem under investigation and then the system operation is explained.
ii) In Section 3, firstly, a brief and useful overview around the modeling and optimization steps is presented and then details of them are described and their related mathematical equations are formulated.
iii) The effort of Section 4 is paid to present the outputs of the modeling and optimization procedures. Before it, the validity of the developed model is firstly demonstrated in this section.
iv) Section 5 is dedicated to concluding remarks, perspective of the study, and suggestions for future works.

Table 2
Final form of the required equations for developing the energy model of the ejector [31].

Description	Equation
Mass entrainment ratio of the ejector	$\mu = \frac{\dot{m}_{SF}}{\dot{m}_{PF}} = \frac{\dot{m}_{13}}{\dot{m}_{12}}$
Energy balance in the nozzle for the primary flow	$u_{PF,N_{out}} = \sqrt{2(h_{PF,N_{in}} - h_{PF,N_{out}})}$
Isentropic efficiency of the nozzle	$\eta_{N,s} = \frac{h_{PF,N_{in}} - h_{PF,N_{out}}}{h_{PF,N_{in}} - h_{PF,N_{out},s}}$
Energy balance in the nozzle for the secondary flow	$u_{SF,N_{out}} = \sqrt{2(h_{SF,N_{in}} - h_{SF,N_{out}})}$
Momentum balance for the mixing chamber	$u_{MF,s} = \frac{u_{PF,N_{out}} + \mu u_{SF,N_{out}}}{1+\mu}$
Efficiency of the mixing chamber	$\eta_M = \frac{u_{MF}^2}{u_{MF,s}^2}$
Energy conservation for the mixing chamber	$h_{MF} = \frac{h_{PF,N_{out}} + \mu h_{SF}}{1+\mu} - \frac{u_{MF}^2}{2}$
Isentropic efficiency of the diffuser	$\eta_{D,s} = \frac{h_{D,s} - h_{MF}}{h_D - h_{MF}}$
Mass entrainment ratio of the ejector based on the ejector's parameters	$\mu = \sqrt{\eta_{N,s}\eta_M\eta_{D,s}(h_{PF,N_{in}} - h_{PF,N_{out},s})/(h_{D,s} - h_{MF})} - 1$
Coefficient of performance for the ERC	$COP = \frac{\text{Produced cooling load in ERC}}{\text{Input heating load to ERC}}$

2. Problem description and system operation

This section gives information about the layout of the system and also its operating strategy. The problem under investigation is around development, modeling, and finding the optimal working operation of a MGES. The system is designed based on the district energy conditions and considered to work as an energy hub. To achieve this goal, this system can supply the power, cooling, and heating demands together with the production of hydrogen (as a clean fuel). An outline of the proposed MGES is drawn in Fig. 1 and the system operation strategy is explained in the following. Also, the following technical assumptions are taken for the system modeling in this study:

- Based on the nature of the system equipment, changes in the velocity and height at the inlet/outlet sections of the equipment are low, except in the EJ. Accordingly, variation of the kinetic energy is neglected in all equipment except in the EJ (the momentum conservation equation should also be applied for the EJ).
- The heat loss from the CC during the combustion reaction is considered by defining thermal efficiency of the CC.
- Based on the nature of the fluid flowing in the cycles, pressure drops for the RGTC's equipment are considered, but it is negligible for the bottoming cycles.
- The fluid flow within the EV is isenthalpic.
- The air entering into the COM is composed of 77.48 % N_2, 20.59% O_2, 1.9% H_2O, and 0.03% CO_2. Natural gas is considered as the injected fuel into the CC and it is assumed to be pure methane (because, in most cases, more than 95%~98% of natural gas is made of methane). Also, depending on the system's operating conditions, the molar fuel–air ratio is calculated within the thermodynamic modeling procedure, and finally solving the combustion reaction results in the components of the flue gas.

The RGTC acts as the primary runner cycle, where the main power of the system is generated and is sold to the power grid, as one of the project incomes. The RGTC is the modified version of the basic GTC, in which an AP is utilized for improving the efficiency of the basic GTC (utilizing the AP causes a hotter air entering into the CC and results in the reduction of fuel consumption in the CC to reach the desirable exhaust gases temperature). In this work, an attempt has been made to maximally utilize the heating potential of hot outflow gas from the GT of the RGTC. For this, a district heating heat exchanger (HEX_1) is firstly inserted on the way of the exhaust gases and the hot water is produced based on the 3GDH (third-generation district heating) conditions. Afterward, the exhaust gases are respectively guided into the VG and HEX_3 for driving the RC and PEMEC. In the RC, some extra power is generated;

Table 3
Final form of the required equations for developing the energy model of the PEM eletrolyzer [32].

Description	Equation
Chemical formula of the water splitting reaction	$H_2O + \text{energy} \rightarrow H_2 + \frac{1}{2}O_2$; $\begin{cases} H_2O \rightarrow 2H^+ + 2e^- + \frac{1}{2}O_2 \ , \ \textit{Anode side} \\ 2H^+ + 2e^- \rightarrow H_2 \ , \ \textit{Cathode side} \end{cases}$
Total required energy for splitting reaction	$\Delta G = \Delta H - T\Delta S$
Molar flow rate of the hydrogen	$\dot{N}_{H_2} = \frac{J}{2F}$
Input power to the electrolyzer	$\dot{W}_{PEME} = JV$
Voltage potential of the electrolyzer	$V = V_0 + V_{act,a} + V_{act,c} + V_{ohm}$
Reversible potential (the Nernst equation)	$V_0 = 1.229 - [8.5 \times 10^{-4}(T_{PEME} - 298)]$
Activation over-potential of the anode	$V_{actv,a} = \frac{RT}{F}\sinh^{-1}\left(\frac{J}{2J_{0,a}}\right)$; $J_{0,a} = J_{ref,a}\exp\left(-\frac{E_{actv,a}}{RT}\right)$
Activation over-potential of the cathode	$V_{actv,c} = \frac{RT}{F}\sinh^{-1}\left(\frac{J}{2J_{0,c}}\right)$; $J_{0,c} = J_{ref,c}\exp\left(-\frac{E_{actv,c}}{RT}\right)$
Ohmic over-potential of the electrolyte	$V_{ohm} = JR_{PEME}$; $\begin{cases} R_{PEME} = \int_0^D \frac{dx}{\sigma_{PEME}(\lambda(x))} \\ \sigma_{PEME}(\lambda(x)) = [0.5139\lambda(x) - 0.326] \times \exp\left[1268\left(\frac{1}{303} - \frac{1}{T_{PEME}}\right)\right] \\ \lambda(x) = \left(\frac{\lambda_a - \lambda_c}{D}\right)x + \lambda_c \end{cases}$

Table 4
Correlations used for determining purchasing cost of the MGES equipment.

Cycle	Equipment name	Purchase equipment cost [$]	Reference
Regenerative gas turbine cycle	Compressor	$PEC_{COM} = \left(\frac{39.5\times\dot{m}_1}{0.9-\eta_{COM,s}}\right)\left(\frac{P_2}{P_1}\right)\left[\ln\left(\frac{P_2}{P_1}\right)\right]$	[36]
	Air pre-heater*	$PEC_{AP} = 2290\times(A_{AP})^{0.6}$	[36]
	Combustion chamber	$PEC_{CC} = \left(\frac{25.6\times\dot{m}_3}{0.995-\frac{P_4}{P_3}}\right)[1+\exp(0.018T_4-26.4)]$	[36]
	Gas turbine	$PEC_{GT} = \left(\frac{266.3\times\dot{m}_4}{0.92-\eta_{GT,s}}\right)\left[\ln\left(\frac{P_4}{P_5}\right)\right][1+\exp(0.036T_4-54.4)]$	[36]
District heating heat exchanger	Heat exchanger 1*	$PEC_{HEX_1} = 12000\times\left(\frac{A_{HEX_1}}{100}\right)^{0.6}$	[37]
	Vapor generator*	$PEC_{VG} = 17500\times\left(\frac{A_{VG}}{100}\right)^{0.6}$	[37]
Rankine cycle	Steam turbine	$PEC_{ST} = 3880.5\times\dot{W}_{ST}^{0.7}\left(1+\left(\frac{0.05}{1-\eta_{ST,s}}\right)^3\right)\left[1+5\exp\left(\frac{T_{20}-866}{10.42}\right)\right]$	
	Heat exchanger 2*	$PEC_{HEX_2} = 12000\left(\frac{A_{HEX_2}}{100}\right)^{0.6}$	[37]
	Pump 2	$PEC_{PU_2} = 2100\left(\frac{\dot{W}_{PU_2}}{10}\right)^{0.26}\times\left(\frac{1-\eta_{PU_2,s}}{\eta_{PU_2,s}}\right)^{0.5}$	[37]
Ejector refrigeration cycle	Ejector	$PEC_{EJ} = 1000\times16.14\times0.989\times\dot{m}_{12}\times\left(\frac{T_{12}}{0.1P_{12}}\right)^{0.05}\times(0.1P_{14})^{-0.75}$	[36]
	Evaporator*	$PEC_{EVA} = 16000\times\left(\frac{A_{EVA}}{100}\right)^{0.6}$	[37]
	Condenser*	$PEC_{CON} = 8000\times\left(\frac{A_{CON}}{100}\right)^{0.6}$	[37]
	Expansion valve	$PEC_{EV} = 114.5\times\dot{m}_{17}$	[37]
	Pump 1	$PEC_{PU_1} = 2100\left(\frac{\dot{W}_{PU_1}}{10}\right)^{0.26}\times\left(\frac{1-\eta_{PU_1,s}}{\eta_{PU_1,s}}\right)^{0.5}$	[37]
PEM elctrolyzer cycle	Heat exchanger 3*	$PEC_{HEX_3} = 12000\left(\frac{A_{HEX_3}}{100}\right)^{0.6}$	[37]
	PEM electrolyzer	$PEC_{PEME} = 1000\dot{W}_{PEME}$	[38]
	Separator	$PEC_{SEP} = 114.5\times\left(\dot{m}_{30}\right)^{0.67}$	[37]

* The required heat transfer area (A) of different heat exchanging equipment in the cycle is calculated based on the material presented in Appendix A.

considering design limitations of PEMEs, half of this extra power is fed to the PEME, and the remaining half is transmitted to the power grid for sale. In the PEMEC, the inlet pre-heated water is split into its constituent elements (the hydrogen and oxygen are respectively produced at the cathode and anode sides of the PEME). The produced hydrogen can be stored in tanks, used in hydrogen vehicles, blended into the NG grid with a permissible concentration (1–10 vol% [27]), or used for producing methane through the utilization of the exhaust gases (carbon capture) in a methanation unit (an attractive application of the proposed MGES for P2G (power to gas) technology, which made the system even cleaner and more sustainable [27]). Furthermore, an ERC is coupled to the RC at the HEX_2 and the cooling load is produced at the EVA based on the 3GDC (third-generation district cooling) conditions.

3. Problem modeling and optimizing procedures

The effort of this section is focused on presenting full details of the modeling and optimization procedures. The analyses in this study are divided into two main sections: (a) problem modeling, and (b) optimal operating conditions. A summary about the modeling and optimizing procedures is depicted in Fig. 2. The program of the problem model is developed in the Engineering Equation Solver (EES) software and the optimization is done through developing a computation code in Matlab software based on the NSGA-II method.

A complete evaluation of MGESs should consist of four different analyses including:

(1) *Energy analysis*: This step begins with the development of the system's thermodynamic model and results in the calculation of the system's energetic outputs (in this study: the net generated power, the produced heating load, the produced cooling load, and mass flow rate of the produced hydrogen). In the present study, a potent thermodynamic model is derived with realistic assumptions for all of the system equipment. The sizing of all cycles (i.e. mass flow rate of working fluids) is variable based on the system's working operation. However, in the majority of previous studies, the system operated with a constant size. It means that, for the sake of simplification, the mass flow rates of the working fluids were assumed to be constant (as the input parameters of the problem) in most of the previous studies.
(2) *Exergy analysis*: This step is based on the second-law of thermodynamics and gives information about the rate of system

Table 5
Final form of the main equations for the eco-exergy model.

Cycle	Equipment name	Exergoeconomic model	Auxiliary equation
Regenerative gas turbine cycle	Compressor	$\dot{C}_2 = \dot{C}_1 + \dot{C}_{W,\mathrm{COM}} + \dot{Z}_{\mathrm{COM}}$	$c_{W,\mathrm{COMP}} = c_{W,\mathrm{GT}} c_1 = 0$
	Air pre-heater	$\dot{C}_3 + \dot{C}_6 = \dot{C}_2 + \dot{C}_5 + \dot{Z}_{\mathrm{AP}}$	$c_6 = c_5$
	Combustion chamber	$\dot{C}_4 = \dot{C}_3 + \dot{C}_{10} + \dot{Z}_{\mathrm{CC}}$	$\dot{C}_{10} = \dot{C}_f = \left(c_f \times \dot{m}_{10} \times \mathrm{LHV}_f\right) \times 3600 \times t_{\mathrm{year}}$
	Gas turbine	$\dot{C}_5 + \dot{C}_{W,\mathrm{GT}} = \dot{C}_4 + \dot{Z}_{\mathrm{GT}}$	$c_5 = c_4$
District heating heat exchanger	Heat exchanger 1	$\dot{C}_7 + \dot{C}_9 = \dot{C}_6 + \dot{C}_8 + \dot{Z}_{\mathrm{HEX_1}}$	$c_7 = c_6 c_8 = 0$
Rankine cycle	Vapor generator	$\dot{C}_{11} + \dot{C}_{20} = \dot{C}_7 + \dot{C}_{23} + \dot{Z}_{\mathrm{VG}}$	$c_{11} = c_7$
	Steam turbine	$\dot{C}_{21} + \dot{C}_{W,\mathrm{ST}} = \dot{C}_{20} + \dot{Z}_{\mathrm{ST}}$	$c_{21} = c_{20}$
	Heat exchanger 2	$\dot{C}_{22} + \dot{C}_{12} = \dot{C}_{21} + \dot{C}_{18} + \dot{Z}_{\mathrm{HEX_2}}$	$c_{22} = c_{21}$
	Pump 2	$\dot{C}_{23} = \dot{C}_{22} + \dot{C}_{W,\mathrm{PU_2}} + \dot{Z}_{\mathrm{PU_2}}$	$c_{W,\mathrm{PU_2}} = c_{W,\mathrm{ST}}$
Ejector refrigeration cycle	Ejector	$\dot{C}_{14} = \dot{C}_{12} + \dot{C}_{13} + \dot{Z}_{\mathrm{EJ}}$	–
	Evaporator	$\dot{C}_{13} + \dot{C}_{27} = \dot{C}_{19} + \dot{C}_{26} + \dot{Z}_{\mathrm{EVA}}$	$c_{13} = c_{19} c_{26} = 0$
	Condenser	$\dot{C}_{15} + \dot{C}_{25} = \dot{C}_{14} + \dot{C}_{24} + \dot{Z}_{\mathrm{CON}}$	$c_{15} = c_{14} c_{24} = 0$
	Expansion valve	$\dot{C}_{19} = \dot{C}_{17} + \dot{Z}_{\mathrm{EV}}$	–
	Pump 1	$\dot{C}_{18} = \dot{C}_{16} + \dot{C}_{W,\mathrm{PU_1}} + \dot{Z}_{\mathrm{PU_1}}$	$c_{W,\mathrm{PU_1}} = c_{W,\mathrm{ST}}$
	Division point	$\dot{C}_{15} = \dot{C}_{16} + \dot{C}_{17}$	$c_{16} = c_{17}$
PEM elctrolyzer cycle	Heat exchanger 3	$\dot{C}_{29} + \dot{C}_{35} = \dot{C}_{11} + \dot{C}_{28} + \dot{Z}_{\mathrm{HEX_3}}$	$c_{35} = c_{11} c_{28} = 0$
	PEME electrolyzer	$\dot{C}_{32} + \dot{C}_{30} = \dot{C}_{34} + \dot{C}_{W,\mathrm{PEME}} + \dot{Z}_{\mathrm{PEME}}$	$c_{W,\mathrm{PEME}} = c_{W,\mathrm{ST}}$
	Separator	$\dot{C}_{31} + \dot{C}_{33} = \dot{C}_{30} + \dot{Z}_{\mathrm{SEP}}$	$\frac{\dot{C}_{31} - \dot{C}_{30}}{\dot{E}_{31} - \dot{E}_{30}} = \frac{\dot{C}_{33} - \dot{C}_{30}}{\dot{E}_{33} - \dot{E}_{30}}$
	Division point	$\dot{C}_{29} + \dot{C}_{31} = \dot{C}_{34}$	–

Table 6
Final form of the main required equations for the enviro-exergy model.

Description	Equation
Real combustion reaction of hydrocarbon $C_{x_1}H_{x_2}$	$\overline{\lambda} C_{x_1} H_{x_2} + (0.2059 O_2 + 0.7748 N_2 + 0.019 H_2O + 0.0003 CO_2) \rightarrow y_{CO_2} CO_2 + y_{N_2} N_2 + y_{O_2} O_2 + y_{H_2O} H_2O + y_{NO} NO + y_{CO} CO$
Equivalence ratio	$\varnothing = \frac{\text{stoichiometric } \overline{\lambda}}{\text{Actual } \overline{\lambda}} \; ; \; \overline{\lambda} = \frac{n_{10}}{n_1}$
Temperature of the combustion chamber primary zone**	$T_{\mathrm{PZ}} = \mathscr{C} \delta^{\kappa} \exp\left(\vartheta(\delta + \varepsilon)^2\right) \left(\frac{P_3}{P_0}\right)^{x^*} \left(\frac{T_3}{P_0}\right)^{y^*} \left(\frac{x_2}{x_1}\right)^{z^*}$
Mass flow of the emitted nitrogen oxide	$m_{\mathrm{NOx}} = \frac{0.15 \times 10^{16} \mathscr{T}^{0.5} \exp(-71100/T_{\mathrm{PZ}})}{P_3^{0.05} (\Delta P_{\mathrm{CC}}/P_3)^{0.5}} \; ; \; \dot{m}_{\mathrm{NOx}} = m_{\mathrm{NOx}} \times 10^{-3} \times \dot{m}_{10}$
Mass flow rate of the emitted carbon monoxide	$m_{\mathrm{CO}} = \frac{0.179 \times 10^{9} \exp(7800/T_{\mathrm{PZ}})}{P_3^{2} \mathscr{T} (\Delta P_{\mathrm{CC}}/P_3)^{0.5}} \; ; \; \dot{m}_{\mathrm{CO}} = m_{\mathrm{CO}} \times 10^{-3} \times \dot{m}_{10}$
Environmental penalty cost rate	$\dot{C}_{\mathrm{env}} = \left[c_{CO_2} \times \dot{m}_{CO_2} + c_{\mathrm{CO}} \dot{m}_{\mathrm{CO}} + c_{\mathrm{NOx}} \dot{m}_{\mathrm{NOx}}\right] \times 3600 \times t_{\mathrm{year}}$

** All details about the constant values in this equation can be found in reference [39].

irreversibility. In the other words, it calculates that how much of the system's exergy is lost during energy conversion processes.

(3) *Environmental analysis*: This step investigates the environmental impact of the system. The conventional environmental analysis just presents the amount of the released pollutants. Furthermore, in most of the previous studies in the field, the combustion process is not addressed for the simplification of the modeling procedure (just pays attention to CO_2). In the present study, all of the main pollutants and greenhouse gases (including CO_2, CO, and NOx) are involved in the modeling procedure. To make the analysis even more fruitful, the enviro-exergy model is presented instead of the conventional environmental analysis. This analysis illustrates the amount of the released harmful gases per system's productions based on the system's working operation.

(4) *Economic analysis*: This step examines whether the implementation of the proposed system is economically viable or not. To have a better understanding, an eco-exergy model is developed, which presents the system costs per system's productions. Furthermore, unlike most previous studies which considered a fixed amount for the equipment cost in terms of their production/consumption scale, accurate correlations are utilized for determining the equipment cost based on the system's working operation.

3.1. Energy and exergy models

The energy and exergy models, which respectively are based on the first- and second-law of thermodynamics, are the initial analyzing tools

Table 7
Required input data for the modeling procedure.

Parameter		Symbol	Value	Reference
Reference temperature/ pressure		T_0/ P_0	289 K/1.01 bar	[4]
Isentropic efficiency of	Compressor	$\eta_{COM,s}$	86%	
	Gas turbine	$\eta_{GT,s}$	86%	
	Steam turbine	$\eta_{ST,s}$	85%	
	Pumps	$\eta_{PU_1,s}$, $\eta_{PU_2,s}$	80%, 80%	
Pressure drop within	Air pre-heater (air side)	$\Delta P_{AP,air}$	5%	
	Air pre-heater (exhaust gases side)	$\Delta P_{AP,gas}$	3%	
	Combustion chamber	ΔP_{CC}	5%	
	Heat exchanger 1 (exhaust gases side)	ΔP_{HEX_1}	5%	
Inlet temperature of combustion chamber		T_3	750 K	
Thermal efficiency of combustion chamber		η_{CC}	98%	
Fuel supply pressure		P_{10}	12 bar	
District heating supply/ return temperature		T_9/ T_8	353 K/313 K	[41]
Isentropic efficiency of ejector's nozzle		$\eta_{N,s}$	85%	[42]
Efficiency of ejector's mixing chamber		η_M	90%	
Isentropic efficiency of ejector's diffuser		$\eta_{D,s}$	85%	
District cooling supply/ return temperature		T_{33}/ T_{32}	281 K/288 K	[41]
Temperature of PEM electrolyzer		T_{34}	353 K	[42]
Thickness of membrane		D	100 μm	
Activation energy of anode/ cathode		$E_{actv,a}$/ $E_{actv,c}$	76 kJ mol^{-1}/ 18 kJ mol^{-1}	
Water content of anode/ cathode		λ_a/ λ_c	14 Ω^{-1}/ 10 Ω^{-1}	
Pre-expotential factor of anode/ cathode		$J_{ref,a}$/ $J_{ref,c}$	1.7×10^5 A m^{-2}/ 4.6×10^3 A m^{-2}	
Faraday constant		F	96,486 C mol^{-1}	
Fuel cost/ lower heating value		c_f/ LHV_f	2.5 \$.GJ^{-1}/ 50916.96 kJ kg^{-1}	
Selling price of	power	c_{power}	30 €.$(MWh)^{-1}$	[41]
	heat	c_{heat}	20 €.$(MWh)^{-1}$	
	cold	c_{cold}	25 €.$(MWh)^{-1}$	
	hydrogen	$c_{hydrogen}$	7 \$ kg^{-1}	
Releasing penalty coefficient of	carbon dioxide	c_{CO_2}	0.024 \$ $kg_{CO_2}^{-1}$	[42]
	carbon monoxide	c_{CO}	0.02086 \$ kg_{CO}^{-1}	
	nitrogen oxide	c_{NOx}	6.853 \$ kg_{NOx}^{-1}	
Operating hours during a year		t_{year}	7000 h	[19]
Expected life span of system		N	15 years	
Operating and maintenance coefficient		Φ	1.06	
Effective interest rate		i_{eff}	10%	
Rate of discount		DR	8%	
Rate of inflation		r	5%	

for any energy system. These two models should be developed for all of the system equipment as written in Eqs. (1) and (2) [28,29].

$$\left(\sum_{in}\left[\dot{m}\left(h+\frac{u^2}{2}+gz\right)\right]_{in,k}\right)+\sum\dot{Q}_k = \left(\sum_{out}\left[\dot{m}\left(h+\frac{u^2}{2}+gz\right)\right]_{out,k}\right)+\sum\dot{W}_k \quad (1)$$

$$\left(\sum_{in}\dot{E}x_{in,k}\right)+\overbrace{\left(\sum\left[1-\frac{T_0}{T_k}\right]\dot{Q}_k\right)}^{\dot{E}x_Q} = \left(\sum_{out}\dot{E}x_{out,k}\right)+\overbrace{\left(\sum\dot{W}_k\right)}^{\dot{E}x_W}+\dot{\Psi}_k \quad (2)$$

in which, the terms $\dot{m}$, h, and u stand for mass flow rate, specific enthalpy, and velocity of the working fluids at different flow streams in the cycle. Also, g, z, $\dot{Q}$, $\dot{W}$, $\dot{E}x$, and $\dot{\Psi}$ show gravitational acceleration, height, heat transfer rate, power, exergy rate, and exergy destruction rate, respectively. The subscripts of "k", "in", "out", and "D" refer to the "equipment k in the cycle", "inlet section of equipment", "outlet section of equipment", and "destruction", respectively.

During the development of these two models, the laws of conservation for mass and momentum are also required. The final form of the mass and momentum conservation is stated as Eqs. (3) and (4), respectively. Furthermore, the exergy rate for each of the flow streams is calculated as the sum of the physical and chemical exergy rates, as expressed in Eq. (5) [30].

$$\sum_{in}\dot{m}_{in,k} = \sum_{out}\dot{m}_{out,k} \quad (3)$$

$$\sum_{in}(\dot{m}u)_{in,k} = \sum_{out}(\dot{m}u)_{out,k} \quad (4)$$

$$\dot{E}x_k = \overbrace{[\dot{m}((h-h_0)-T_0(s-s_0))]_k}^{\dot{E}x_{ph,k}} + \overbrace{\left[\dot{m}\left(\sum_i Y_i ex_{Ch,i}+\overline{R}T_0\sum_i Y_i lnY_i\right)\right]_k}^{\dot{E}x_{ch,k}} \quad (5)$$

In the above-equations, s is specific entropy, ex is specific exergy, $\overline{R}$=8.314 kJ/kmol.K is the universal gas constant, and the subscript "0″ refers to the reference thermodynamic conditions (i.e. $T_0 = 298$ K and $P_0 = 1.01$ bar).

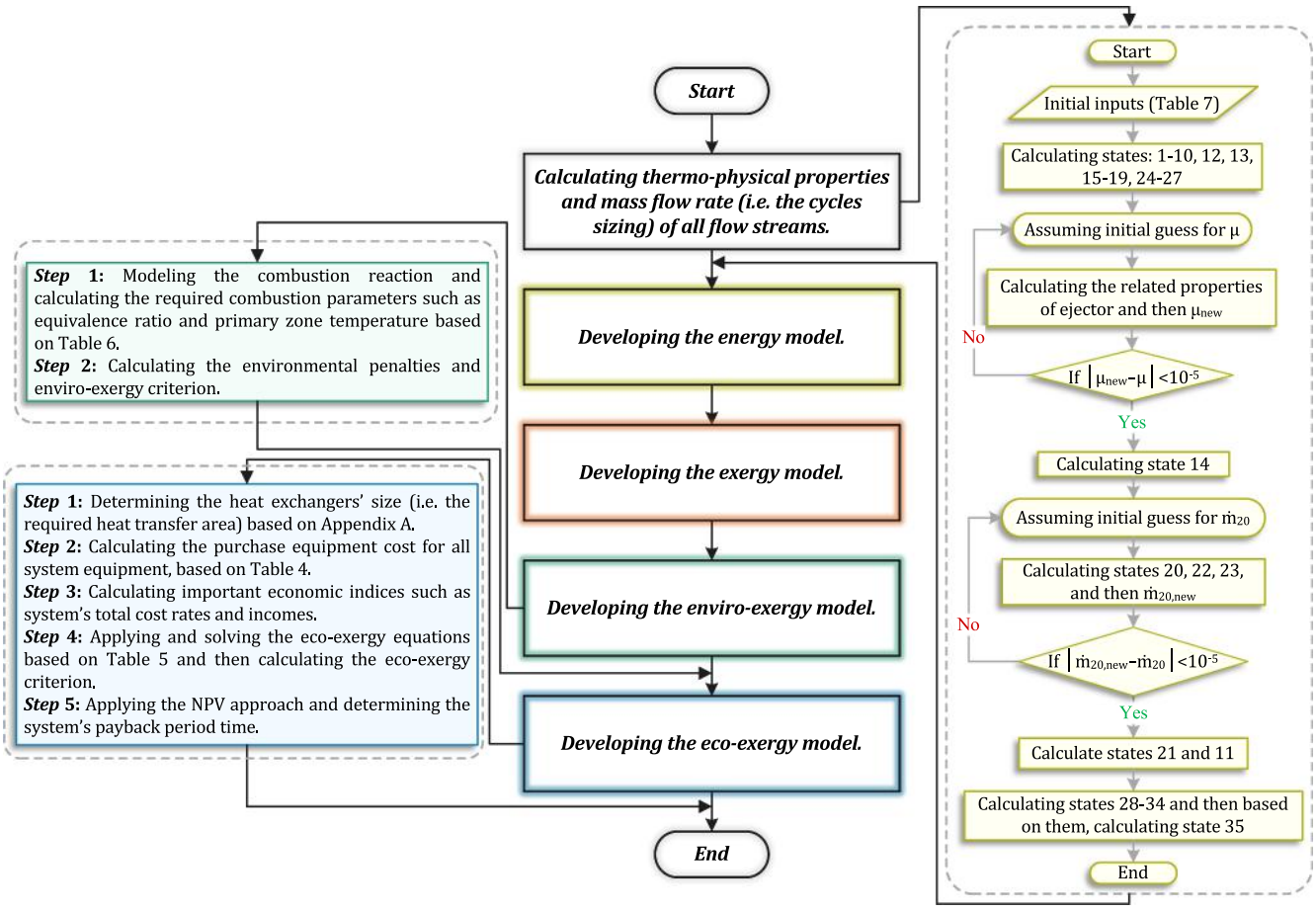

Fig. 3. A flowchart for different steps of the modeling procedure.

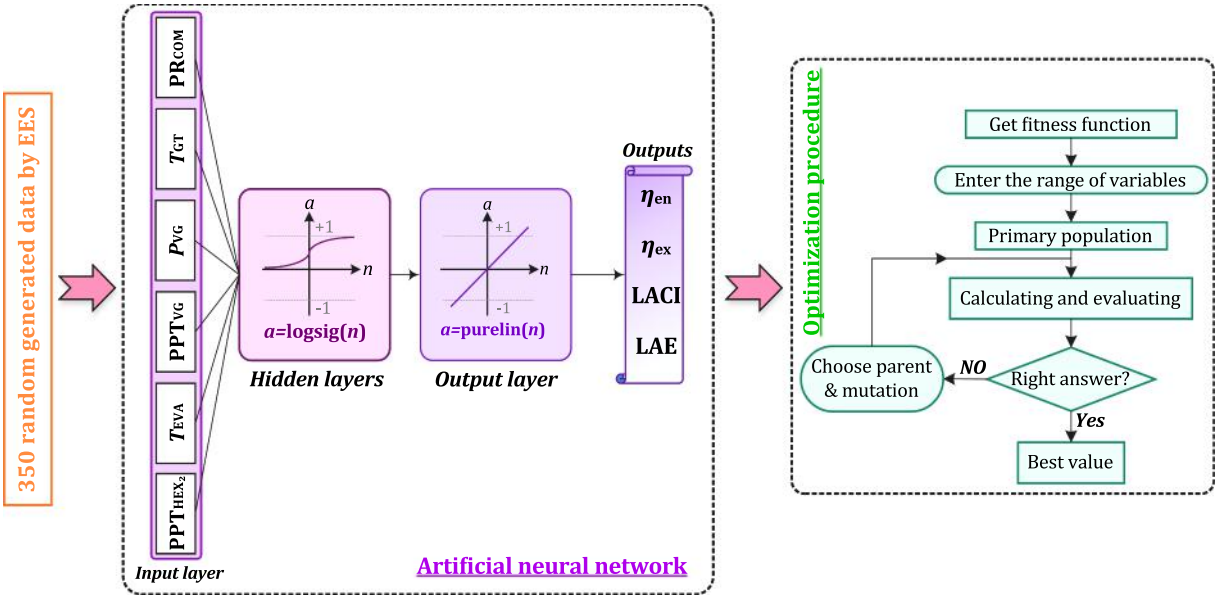

Fig. 4. An illustrative sketch for the methodology of the optimization procedure.

Table 8
List of the assumptions and adjusted values for the ANN and NSGA-II specifications.

Method	Specification	Assumption or adjusted value
ANN	Network architecture	Feed-forward
	Network training approach	Levenberg-Marquardt back-propagation
	Number of hidden layers	2 layers
	Number of neurons in each hidden layer	In the first hidden layer: 5 neurons In the second hidden layer: 4 neurons
	Transfer functions	In the hidden layers: log-sigmoid (logsig) In the output layer: linear (purelin)
	The amount of data used from data bank in different sections in the design of ANN	For training: 70% For validation: 15% For testing: 15%
NSGA-II	Chromosome number of each individual	6
	Individuals number of the population	150
	Maximum iteration number	200
	Mutation probability	0.7
	Crossover probability	0.3

Applying the energy and exergy governing equation to each of the system equipment, the final simplified format of them is listed in Table 1. Furthermore, the energy models of the EJ and PEME are tabulated in Tables 2 and 3, due to the complexity of their model.

3.2. Eco-exergy and enviro-exergy models

As mentioned, the economic feasibility of implementing the proposed plant and its environmental aspects are essential steps that should be taken into account after the confirmation of the system efficiency. For this, the eco-exergy and enviro-exergy models are developed in this study. For each of these two models, real assumptions and robust approaches are utilized as described in the following.

The eco-exergy model is based on solving the equation of cost balance per unit exergy for all system equipment simultaneously. The cost rate balance equation of the equipment k is written as Eq. (6) [33].

$$\left(\sum_{\text{in}}\dot{C}_{\text{in},k}\right)+\left(\sum\dot{C}_{Q,k}\right)+\dot{Z}_k=\left(\sum_{\text{out}}\dot{C}_{\text{out},k}\right)+\left(\sum\dot{C}_{W,k}\right) \tag{6}$$

in which, the parameter $\dot{C}=c\dot{\text{E}}\text{x}$ signifies to the cost rate of flow streams (c is the cost per unit exergy). Hence, the eco-exergy equation (i.e. the equation of cost balance per unit exergy) for the equipment k is obtained as Eq. (7). Also, $\dot{Z}_k$ represents the total non-exergetic cost rate of equipment k (includes purchasing and O&M[2] costs) which is defined as Eq. (8) [34].

$$\left(\sum_{\text{in}}\left[c_{\text{in}}\dot{\text{E}}\text{x}_{\text{in}}\right]_k\right)+\left(\sum\left[c_Q\dot{\text{E}}\text{x}_Q\right]_k\right)+\dot{Z}_k = \left(\sum_{\text{out}}\left[c_{\text{out}}\dot{\text{E}}\text{x}_{\text{out}}\right]_k\right)+\left(\sum\left[c_W\dot{\text{E}}\text{x}_W\right]_k\right) \tag{7}$$

$$\dot{Z}_k=\dot{Z}_k^{\text{PEC}}+\dot{Z}_k^{\text{O\&M}}=\text{PEC}_k\times\text{CRC}\times\Phi \tag{8}$$

where the parameters CRC and Φ denote cost recovery coefficient and O&M coefficient, respectively. These two coefficients are respectively exerted for converting cost [$] to cost rate [$/yr] and for considering yearly O&M costs [35]. Also, precise correlations are employed to determine the purchasing cost of the system equipment (i.e. PEC) based on their operating conditions (refer to Table 4).

[2] O&M: Operating & Maintenance

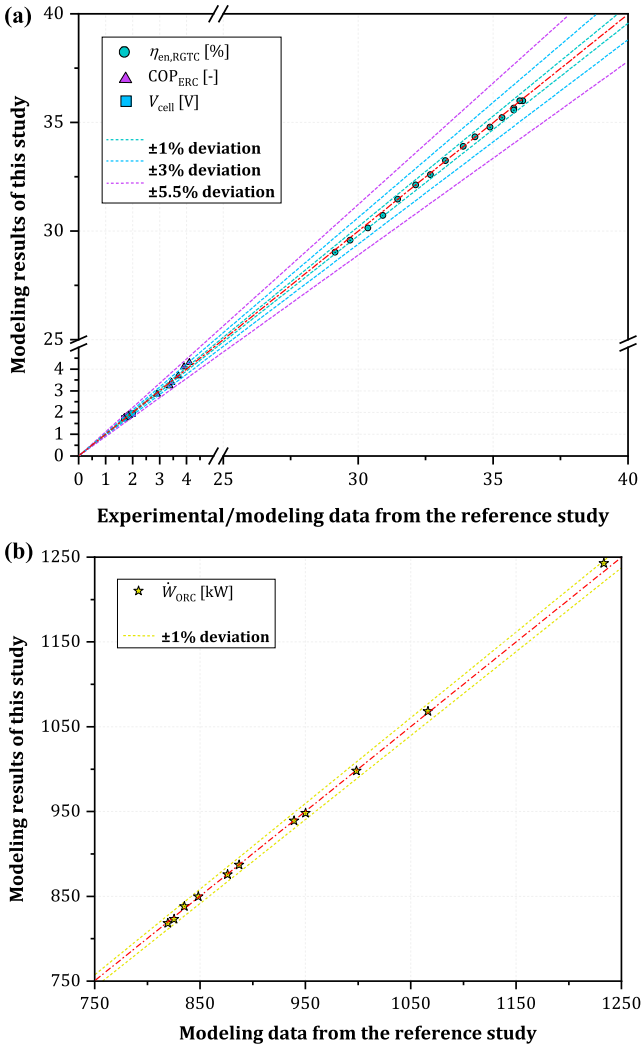

Fig. 5. Validating the results of the modeling procedure in this study versus, (a) modeling results of Moghimi et al. ($\eta_{\text{en,RGTC}}$ for RGTC) [36], experimental results of Yapıcı et al. (COP_{ERC} for ERC) [44], experimental results of Ioroi et al. [45] (V_{cell} for PEMEC), (b) modeling results of Nemati et al. ($\dot{W}_{\text{ORC}}$ for ORC) [43].

$$\text{CRC}=i_{\text{eff}}\times\left[\frac{(1+i_{\text{eff}})^N}{(1+i_{\text{eff}})^N-1}\right] \tag{9}$$

in which, i_{eff} and N imply to the effective interest rate and the system's life span (expected operating years), respectively.

The final simplified format of the eco-exergy and enviro-exergy governing equations are respectively tabulated in Tables 5 and 6.

As another useful result for the economic verification of the proposed MGES, the net present value (NPV) is also calculated and the required time for recovering the initial investment is estimated. In this study, the dynamic payback period is taken into account. Unlike the static payback period (which is not a reliable approach and is just a simple economic technique for doing a quick evaluation), the dynamic approach contains more economic considerations. The static approach has two weaknesses: (i) it does not consider the money which will be saved after the PBP has finished, (ii) it does not take into account the inflation indicators. The effects of inflation and capital discount in each year during the system's life span are taken into consideration in the employed NPV approach and finally, the payback period time is determined [40]:

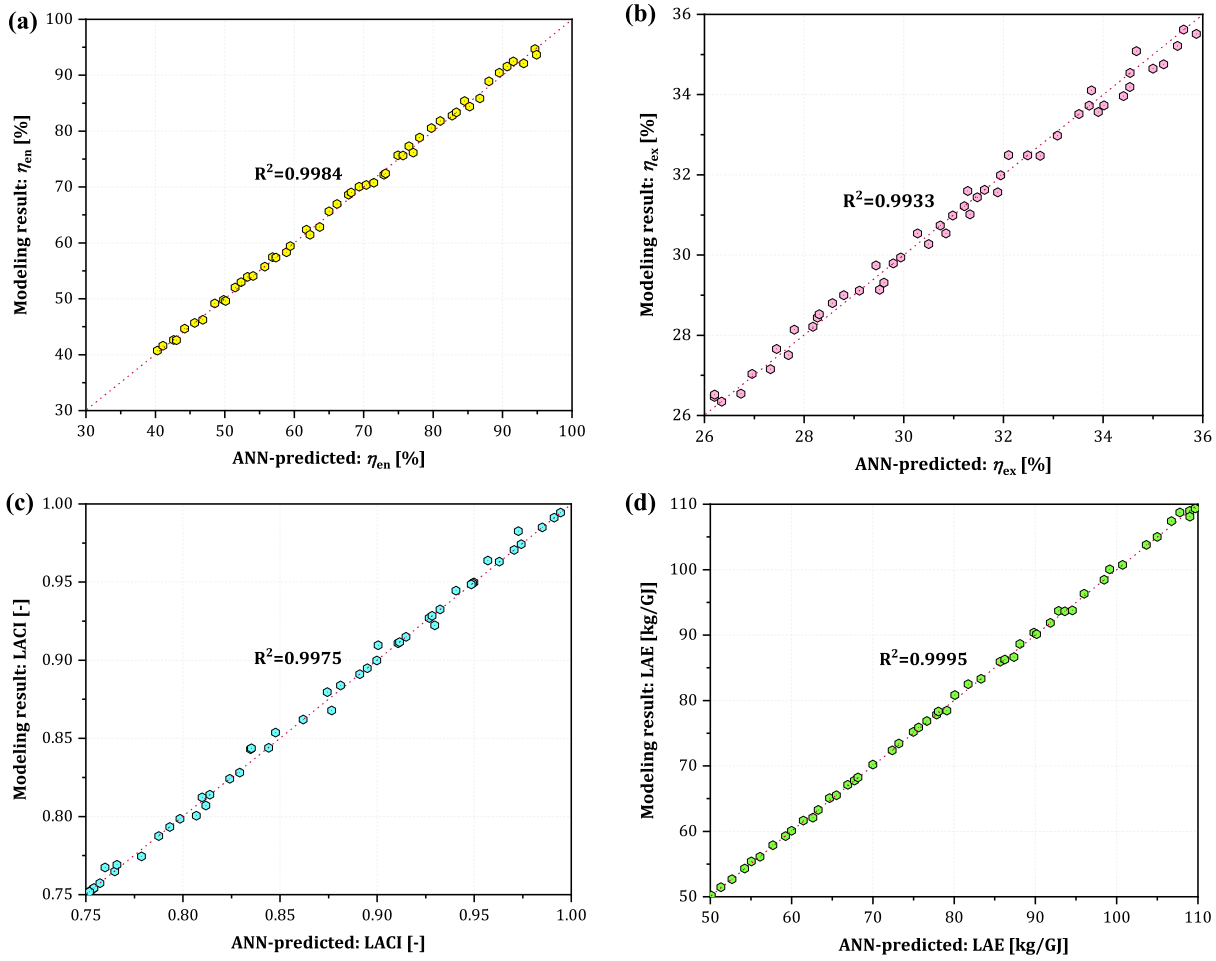

Fig. 6. Verifying the accuracy of the ANN in the prediction of the modeling results for, (a) energy efficiency, (b) exergy efficiency, (c) levelized annual costs to incomes, (d) levelized annual emissions.

$$\begin{cases} \mathrm{NPV}_0 = -(\mathrm{FC} \times \mathrm{IF}_0 \times \mathrm{RDF}_0) \\ \mathrm{NPV}_i = \mathrm{NPV}_{i-1} + (\mathrm{AS} \times \mathrm{IF}_i \times \mathrm{RDF}_i)\ ;\ i = 1, 2, \cdots, N \end{cases} \tag{10}$$

in which, the parameter AS refers to the annual savings which can be calculated by subtracting the annual incomes from annual operating costs. Also, IF and RDF respectively return to the inflation factor and real discount factor which are expressed as follows [50]:

$$\mathrm{IF}_i = \left(1 + \frac{r}{100}\right)^{-i} \tag{11}$$

$$\mathrm{RDF}_i = \left(1 + \frac{\mathrm{RIR}}{100}\right)^{-i} \tag{12}$$

$$\mathrm{RIR} = \mathrm{DR} - r \tag{13}$$

in which, *r,* RIR, and DR refer to the rate of inflation, real interest rate, and discount rate, respectively.

3.3. Assessment criteria, design variables, and input data

As the final step in the modeling procedure, some criteria should be defined to assess the performance of the proposed MGES based on the different developed models. Hence, five assessment criteria are defined namely energy efficiency (η_{en}), exergy efficiency (η_{ex}), levelized cost of productions (LCP), levelized annual emissions (LAE), and levelized annual costs to incomes (LACI). These functions are defined as follows:

$$\eta_{en} = \frac{\text{Total produced energy}}{\text{Total input energy}} = \frac{\dot{W}_{net} + \overbrace{\dot{Q}_{HEX_1}}^{\dot{Q}_{heating}} + \overbrace{\dot{Q}_{EVA}}^{\dot{Q}_{cooling}} + \overbrace{\left(\dot{m}_{32} \times \mathrm{LHV}_{H_2}\right)}^{\dot{E}_{hydrogen}}}{\dot{m}_{10} \times \mathrm{LHV}_f} \tag{14}$$

$$\eta_{ex} = \frac{\text{Total produced exergy}}{\text{Total input exegy}} = \frac{\overbrace{\dot{W}_{net}}^{\dot{E}x_{power}} + \overbrace{\left(\dot{E}x_9 - \dot{E}x_8\right)}^{\dot{E}x_{heating}} + \overbrace{\left(\dot{E}x_{27} - \dot{E}x_{26}\right)}^{\dot{E}x_{cooling}} + \overbrace{\left(\dot{E}x_{32} + \dot{E}x_{30}\right)}^{\dot{E}x_{hydrogen}}}{\dot{E}x_1 + \dot{E}x_{10} + \dot{E}x_{28}} \tag{15}$$

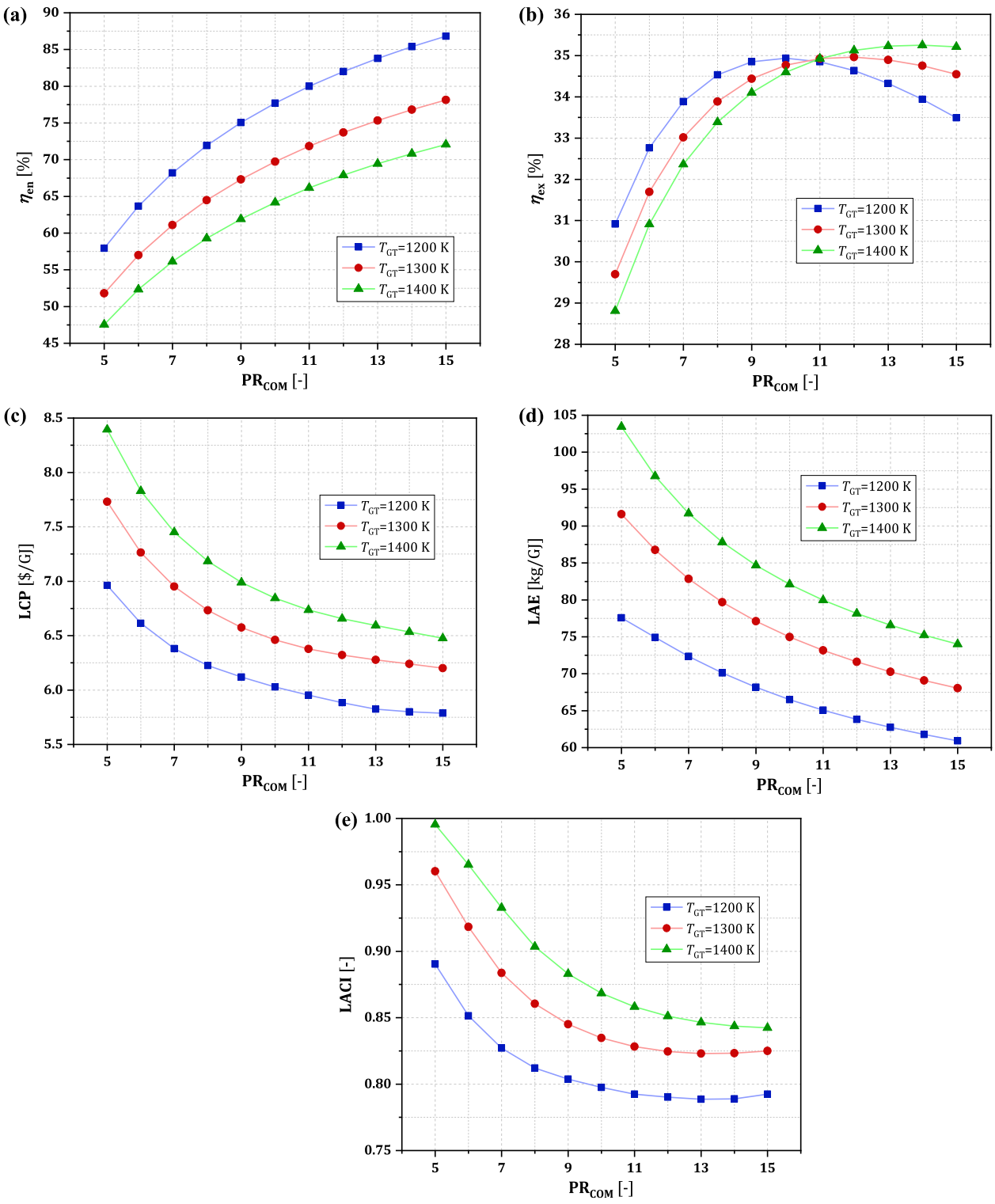

Fig. 7. Variation of the defined assessment criteria in terms of compressor pressure ratio at various gas turbine inlet temperatures.

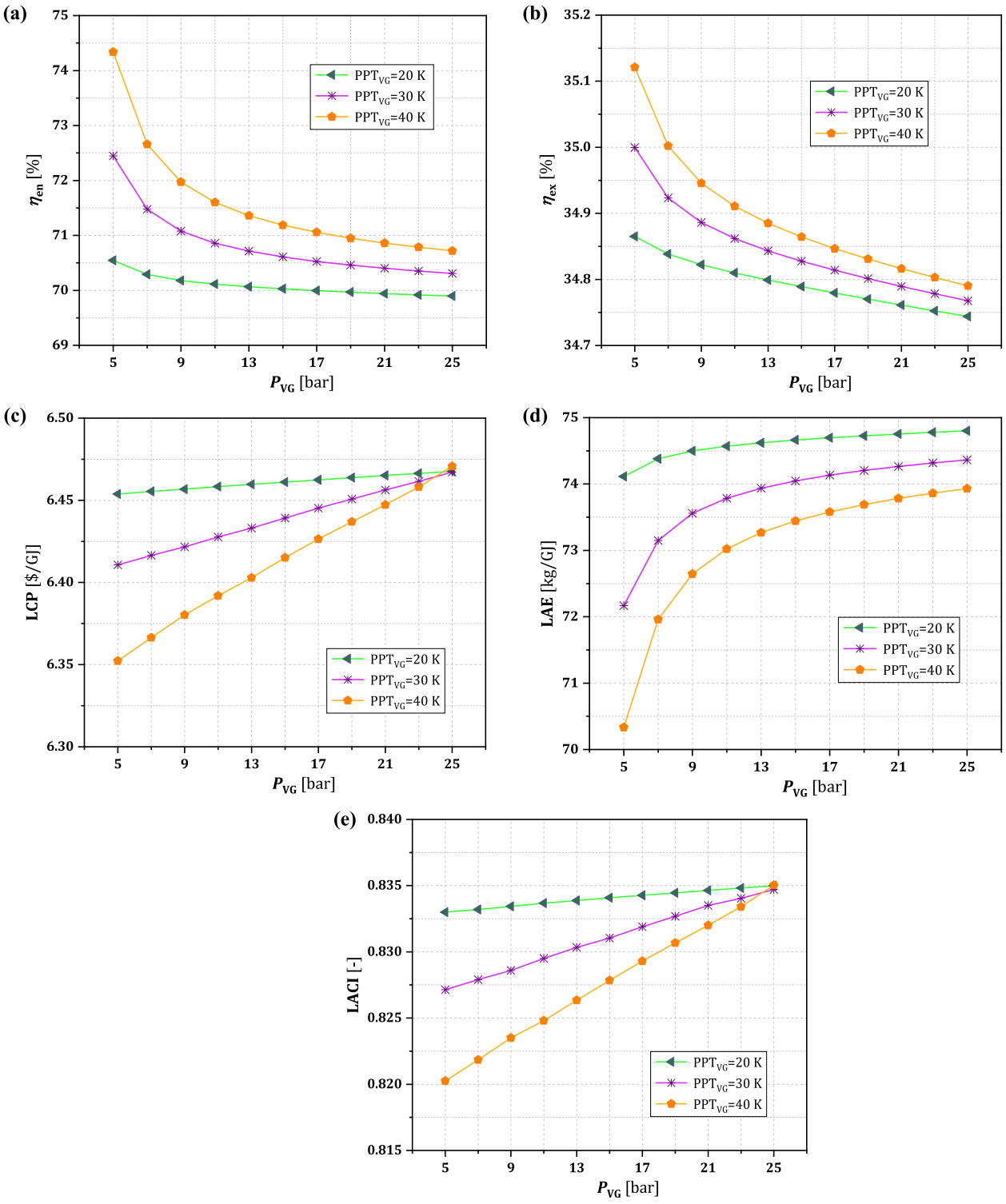

Fig. 8. Variation of the defined assessment criteria in terms of vapor generator pressure at various vapor generator pinch point temperatures.

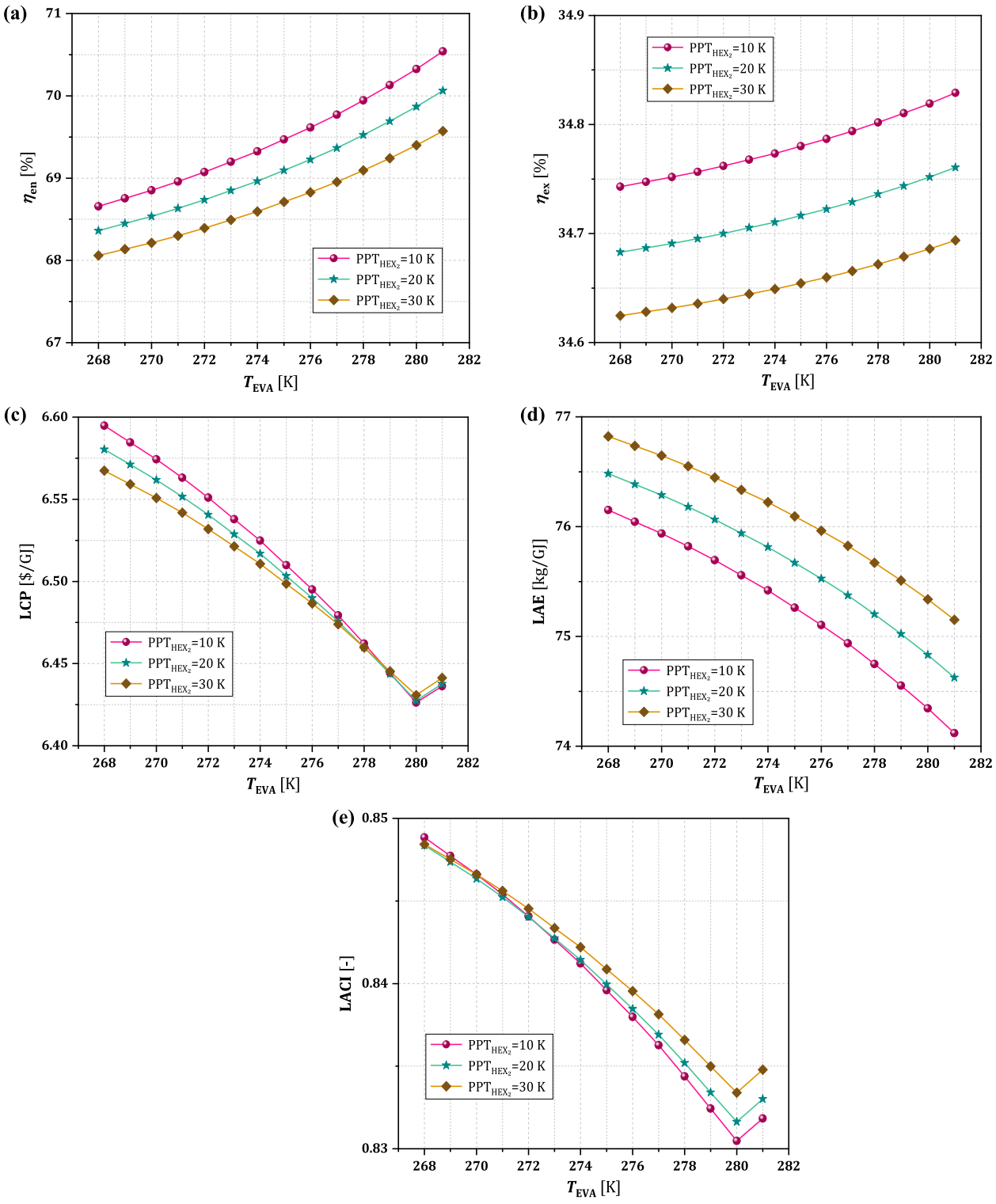

Fig. 9. Variation of the defined assessment criteria in terms of evaporator temperature at various heat exchanger 2 pinch point temperatures.

$$\mathrm{LCP}=\frac{\text{Total annual cost rates}}{\text{Total produced exergy}}=\frac{\overbrace{\dot{C}_{W,\mathrm{net}}}^{\dot{C}_{\mathrm{power}}}+\overbrace{\dot{C}_{9}}^{\dot{C}_{\mathrm{heating}}}+\overbrace{\dot{C}_{27}}^{\dot{C}_{\mathrm{cooling}}}+\overbrace{\left(\dot{C}_{32}+\dot{C}_{30}\right)}^{\dot{C}_{\mathrm{hydrogen}}}}{\left[\dot{\mathrm{Ex}}_{\mathrm{power}}+\dot{\mathrm{Ex}}_{\mathrm{heating}}+\dot{\mathrm{Ex}}_{\mathrm{cooling}}+\dot{\mathrm{Ex}}_{\mathrm{hydrogen}}\right]\times t_{\mathrm{year}}\times 3600} \tag{16}$$

$$\mathrm{LACI}=\frac{\text{Total annual cost rates}}{\text{Total annual incomes}}=\frac{\overbrace{\dot{C}_{W,\mathrm{net}}}^{\dot{C}_{\mathrm{power}}}+\overbrace{\dot{C}_{9}}^{\dot{C}_{\mathrm{heating}}}+\overbrace{\dot{C}_{27}}^{\dot{C}_{\mathrm{cooling}}}+\overbrace{\left(\dot{C}_{32}+\dot{C}_{30}\right)}^{\dot{C}_{\mathrm{hydrogen}}}}{\left[\left(\dot{W}_{\mathrm{net}}\times c\right)+\left(\dot{\mathrm{Ex}}\times c\right)_{\mathrm{heating}}+\left(\dot{\mathrm{Ex}}\times c\right)_{\mathrm{cooling}}+\left(\dot{\mathrm{Ex}}\times c\right)_{\mathrm{hydrogen}}\right]\times t_{\mathrm{year}}} \tag{17}$$

$$\mathrm{LAE}=\frac{\mathrm{Totalannaualemissions}}{\mathrm{Totalproducedexergy}}=\frac{\dot{m}_{\mathrm{CO_2}}+\dot{m}_{\mathrm{CO}}+\dot{m}_{\mathrm{NOx}}}{\dot{\mathrm{Ex}}_{\mathrm{power}}+\dot{\mathrm{Ex}}_{\mathrm{heating}}+\dot{\mathrm{Ex}}_{\mathrm{cooling}}+\dot{\mathrm{Ex}}_{\mathrm{hydrogen}}} \tag{18}$$

In this study, a comprehensive parametric study is conducted to clarify the sensitivity of the assessment criteria to some of the most important design variables of the proposed MGES. The studied design variables include the compressor pressure ratio, gas turbine inlet temperature, vapor generator pressure, vapor generator pinch point temperature, evaporator temperature, and heat exchanger 2 pinch point temperature, with the corresponding investigated range of $5\leq \mathrm{PR_{COM}}$ [-]≤ 15, $1200 \leq T_{\mathrm{GT}}$[K]$\leq 1400$, $5\leq P_{\mathrm{VG}}$[bar]≤ 25, $20\leq \mathrm{PPT_{VG}}$[K]≤ 40, $268\leq T_{\mathrm{EVA}}$[K]≤ 280, and $10\leq \mathrm{PPT_{HEX_2}}$[K]$\leq 30$, respectively. It should be noted that these ranges are the widest ranges based on the technical and thermodynamic possibility of the system and commercial availability of the utilized technologies.

The remaining part of this sub-section presents the initial input data used for the modeling procedure. The list of input data is summarized in Table 7.

A comprehensive flowchart is depicted in Fig. 3 for summarizing all of the steps of the problem modeling procedure. As presented in previous sections and can be inferred from this flowchart, the cycles' sizing (i.e. mass flow rate of the working fluids) and heat exchangers sizing (i.e. the required heat transfer area) varies based on the system's operating conditions. This is while constant values were considered for these two concepts in most of the other similar works. Different steps of the 4E models are done through developing a computational code in EES software. Also, the data library of the EES is used for determining the thermo-physical properties of the flow streams.

Table 9
Optimal operating conditions of the proposed MGES.

Measured item	Optimal amount
Design variables	
$\mathrm{PR_{COM}}$	12.75
T_{GT}	1260
P_{VG}	5.8 bar
$\mathrm{PPT_{VG}}$	29.94 K
T_{EVA}	281 K
$\mathrm{PPT_{HEX_2}}$	10.02 K
Evaluation criteria	
η_{en}	89.75%
η_{ex}	35.21%
LACI	0.756
LAE	58.79 kg/GJ
MGES*'s productions*	
$\dot{W}_{\mathrm{net}}$	21.42 MW
$\dot{Q}_{\mathrm{heating}}$	26.81 MW
$\dot{Q}_{\mathrm{cooling}}$	8.89 MW
$\dot{m}_{\mathrm{H_2}}$	11.96 kg/h

3.4. Optimization model

As the EES software does not support MCO problem, in this study, the optimization is done by the MATLAB software. Therefore, for optimizing the problem, the developed EES code should be called in MATLAB.

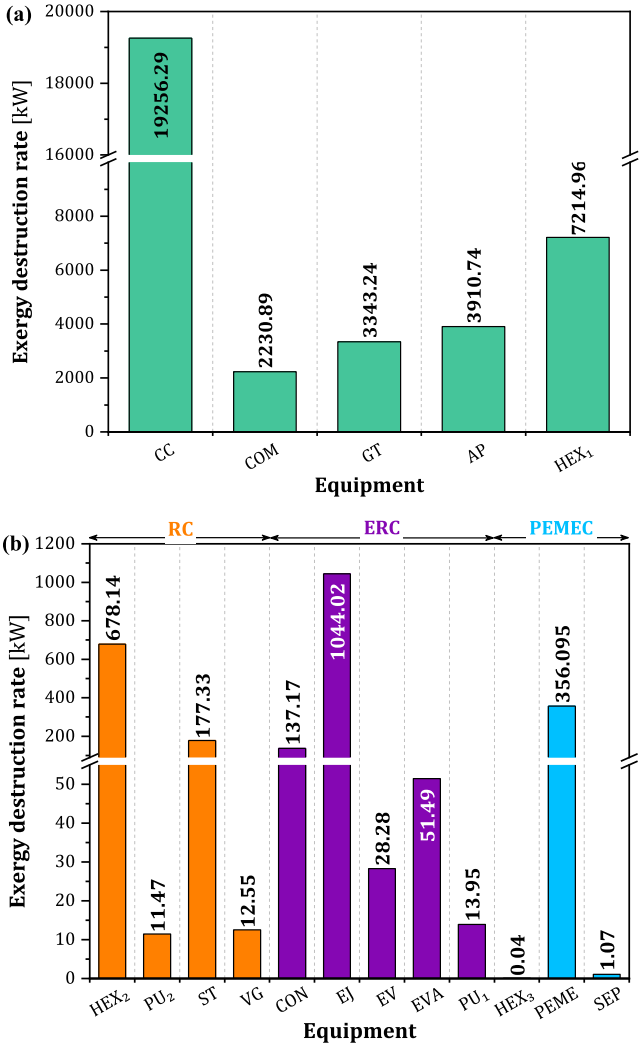

Fig. 10. The exergy destruction rate at the optimal operating conditions for equipment of (a) mover cycle, (b) bottoming cycles.

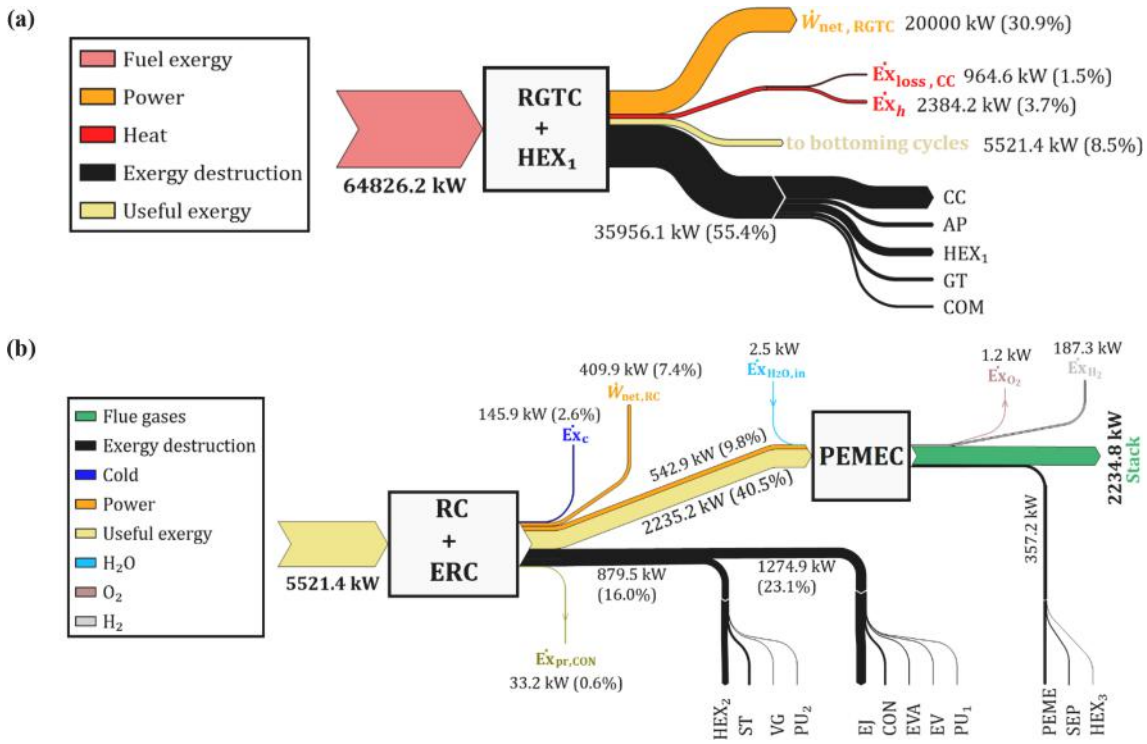

Fig. 11. The Grassmann diagram at the optimal operating conditions for (a) mover cycle, (b) bottoming cycles.

Performing this procedure takes a long calculation time. In this study, an AAN is trained to overcome this issue. In this way, the ANN re-models the problem modeling procedure to make the outputs directly usable in MATLAB. For this, a random data bank (including 350 randomly generated data), including the defined design variables and assessment criteria, is generated by the EES. These data are imported into the ANN for fitting the changing trend of the assessment criteria. Finally, the outputs of the ANN are introduced to the NSGA-II method for reaching the optimal operation of the MGES. This procedure is depicted in Fig. 4 and the specifications of the utilized ANN and NSGA-II are listed in Table 8. It should be mentioned that the ranges of optimization parameters (i.e. the design variables) are the same as that for the parametric study which are presented in the previous section.

4. Results and discussion

This section, firstly, starts with validating the accuracy of the modeling procedure and then continues with presenting a strong parametric study. Finally, the optimal operating conditions of the MGES are sought by applying a MCO procedure.

4.1. Validation and verification of the modeling and optimizing procedures

Due to the novelty of the proposed system layout in this study, this concept has not been studied in the literature. Hence, each sub-cycle is validated through the comparison of its outputs with a reliable recently published work in the field. For this purpose, the modeling results of this study are compared with results of Moghimi et al. (for RGTC) [36], Nemati et al. (for ORC) [43], Yapıcı et al. (for ERC) [44], and Ioroi et al. [45] (for PEMEC). The relative deviation percentage[3] [46] is utilized to express the amount of differences. Based on Fig. 5, the relative deviation percentages are within ±1%, ±1%, ±5.5%, and ±3% for the RGTC, ORC, ERC, and PEMC, respectively. Also, for further verification, the mean absolute error (MAE)[4] is also calculated. Based on Fig. 5, the MAEs are 0.0917, 2.0514, 0.1082, and 0.0192 for the RGTC, ORC, ERC, and PEMC, respectively. Relying on these contents, it can be stated that the results of the modeling procedure are valid and truthful.

In the next step, the accuracy of the ANN-predicted values for the assessment criteria are compared with those of the modeling results. The outputs of this comparison are plotted in Fig. 6 and the coefficient of determination (R^2) is applied for the accuracy evaluation. The results showed that the value of R^2 is 0.9984, 0.9933, 0.9975, and 0.9995 for the η_{en}, η_{ex}, LACI, and LAE, respectively. The closer R^2 values to the unity, the higher the accuracy of the ANN in the prediction of modeling results ($R^2 = 1$ means that the ANN-predicted values exactly match the modeling results). Consequently, the findings demonstrate that the trained ANN is accurate enough.

4.2. Outputs of the modeling procedure (parametric study)

After validating the correctness of the modeling outputs, in this section, a robust and comprehensive parametric study is firstly carried out for analyzing the sensitivity of the system performance to the design variables.

To better present and interpret the outcomes of the parametric study, the most important results are discussed as follows. It is worth mentioning that, in the parametric study, for evaluating the effect of each design variable, the intended variable is varied within its range while the other variables are kept constant.

- The effects of the most important parameters of the RGTC (i.e. PR_{COM} and T_{GT}) are plotted in Fig. 7.

  Analyzing the results illustrated that choosing larger compressors (i.e. higher PR_{COM}) initially leads to warmer air entering the combustion chamber (i.e. higher T_3); but after a certain amount of PR_{COM} (which depends on the amount of other design variables), this trend is reversed. According to the operating strategy of the system under

[3] $\text{Relativedeviationpercentage} = \left(\frac{\text{Presentstudy}-\text{Referencestudy}}{\text{Referencestudy}}\right) \times 100$

[4] $\text{Meanabsoluteerror} = \frac{\sum_{i=1}^{n}|\text{Presentstudy}-\text{Referencestudy}|}{n}$; $n$isnumberofdatapoints

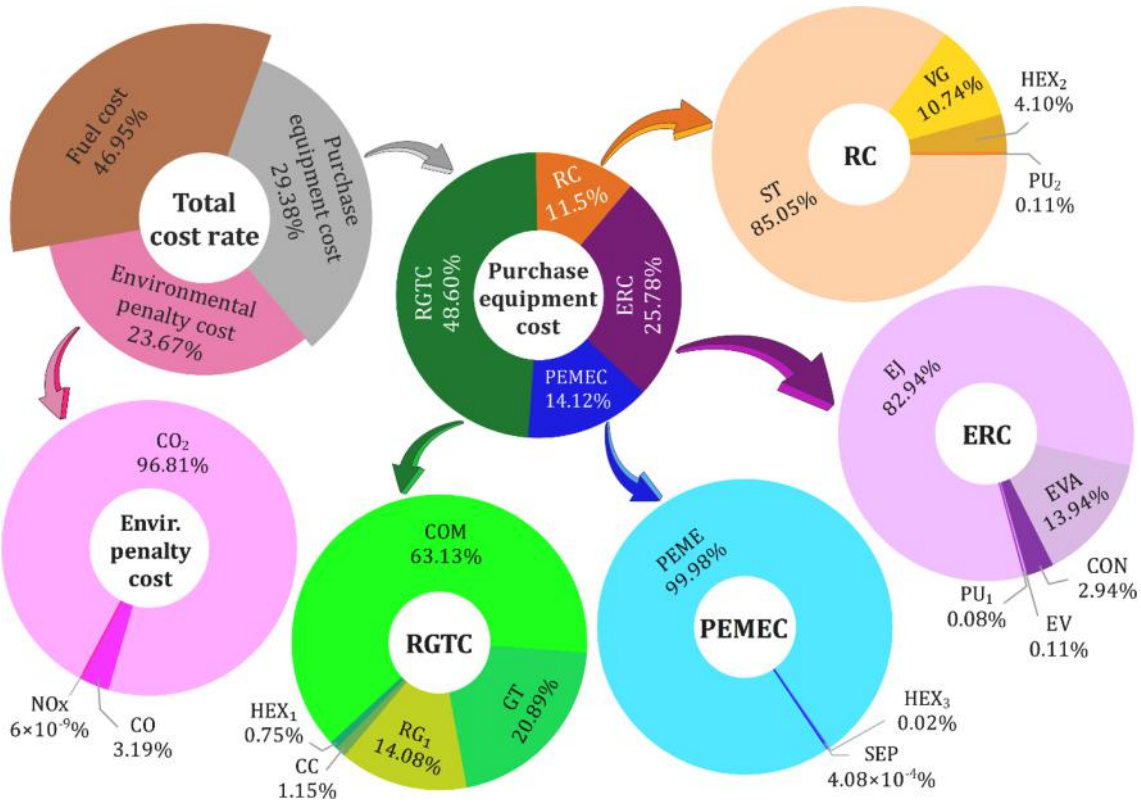

Fig. 12. Cost rate distribution at the optimal operating conditions including all the eco-environmental indices for different cycles and equipment.

study, the higher the temperature of the inlet air to the combustion chamber, the less fuel needs to be injected to achieve the desired T_{GT}. As a conclusion, within the investigated range of PR_{COM}, increasing PR_{COM} initially increases the exergy efficiency, but from a certain amount of PR_{COM} onwards, these trends are reversed. Analyzing the results demonstrated that the variation trend for total pollutants mass flow rate is based on a quadratic polynomial with a minimum point. On the other side, higher PR_{COM} results in the continuous increment of the total productions exergy. The order-of-magnitude for increment of the total produced exergy is very much higher than that of for pollutants rate, and hence it has dominant effect. Based on these behaviors and considering Eq. (18), a continuous reduction trend is observed in enviro-exergy criterion (i.e. LAE) with increasing PR_{COM}. A similar trend is also observed for LCP with the variation of PR_{COM}.

Scrutiny of results showed that the system's total productions, total produced exergy, and total capital costs are consciously increased by the increment of PR_{COM}. But from the other side, for the system's fuel consumption, total fuel exergy, and total emissions rate a minimum point is observed by the variation of PR_{COM} within the studied range.

The parametric study of T_{GT} illustrates that the system's total productions, total produced exergy, and total capital costs are consciously reduced by increment of T_{GT}. But for the other influential criteria (i.e. system's fuel consumption, total fuel exergy, and total emissions rate), the pattern of T_{GT} variations depend on the amount of PR_{COM}. So that, at lower values of PR_{COM}, these three parameters are firstly increased; but as PR_{COM} gets higher, from a certain amount of PR_{COM} onwards, they take a decreasing trend.

Considering the above explanations and taking into account Eqs. (14)–(17), the design variables of RGTC have conflicting effects on the assessment criteria. So that, the final trend of the assessment criteria depends on the effect of the dominant variable (i.e. higher order-of-magnitude). In such a situation, finding the optimal system operating conditions, in which all the assessment criteria are

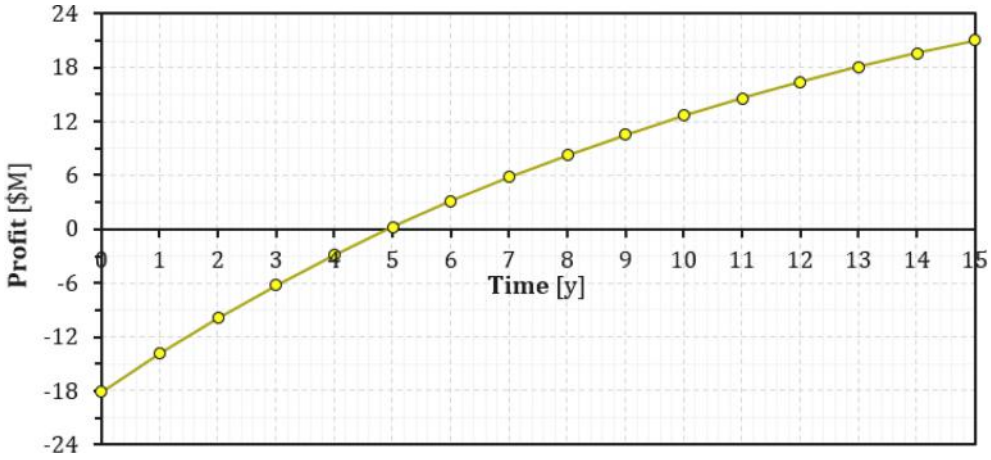

Fig. 13. The net present value at the optimal operating conditions during the system working years.

simultaneously at a desirable value, would be considered as a fruitful finding.

- Unlike the RGTC, changes in the design variables of the bottoming sub-cycles do not have complicated interactions on the evaluation indicators.

  At a certain PPT_{VG}, increasing P_{VG} worsens both of the energy and exergy efficiencies and leads to higher system costs. On the other side, at a certain P_{VG}, adjusting a lower PPT for the VG results in a better performance from all of the energetic, exergetic, and economic standpoints (Fig. 8). So that increasing P_{VG} from 5 bar to 25 bar results a maximum increment of 1.9% in LCP, which is occurred at$PPT_{VG} = 40$ K.

  Also, considering the results of Fig. 9, the increment of T_{EVA} and reduction of PPT_{HEX_2} results in a more efficient system from all of the 4E points-of-view.

- For design parameters of the bottoming cycles, the net generated power is significantly depended on $\dot{W}_{ST}$. Because variation of them have no effect on the power generation of the RGTC, and among the ST and PUs, the $\dot{W}_{ST}$ has a much larger order-of-magnitude.

  For example, increasing P_{VG} results in the reduction of $\dot{W}_{ST}$ and $\dot{W}_{PU_1}$ together with the increment of $\dot{W}_{PU_2}$. As increment of $\dot{W}_{ST}$ has a dominant effect, the general trend of $\dot{W}_{net}$ is in accordance to $\dot{W}_{ST}$ ($\dot{W}_{ST} \gg \left(\dot{W}_{PU_1}, \dot{W}_{PU_2}\right)$). About the reason of reducing trend in $\dot{W}_{ST}$ with increasing P_{VG}, it should be noted that the order-of-magnitude in the reduction of steam mass flow rate passing the ST (i.e. $\dot{m}_{20}$) is dominant over the increment of enthalpy drop within the ST (i.e. $\Delta h = h_{20} - h_{21}$).

- Considering Fig. 8d and Fig. 9d, although the pollutants emission rate does not change with the design variables of the bottoming sub-cycles, they affect the enviro-exergy assessment criteria. Based on the findings discussed above and taking into account Eq. (17), reducing P_{VG}, increasing PPT_{VG}, reducing PPT_{HEX_2}, and increasing T_{EVA} within their studied range lead to a maximum reduction of 4.9%, 5.1%, 1.4%, and 2.7% in LAE. This is while that changing these design variables has no effect on the emitted harmful gases (i.e. $\dot{m}_{CO_2}$, $\dot{m}_{CO}$, and $\dot{m}_{NOx}$ remain constant). This proves the superiority of the enviro-exergy analysis versus conventional environmental analysis.
- Comparing all the results of the parametric study illustrated that the design variables of the RGTC and ERC have the highest and lowest impact on the assessment criteria, respectively.

4.3. Outputs of the optimization procedure (optimal operation)

In the last part of this section, the endeavor is focused on discovering the optimal values of the design variables and operating conditions of the MGES. Since the optimization of the present problem consists of four objective functions (the defined assessment criteria), finding an optimal solution to such MCO problems does not make sense. In this case, there is a so-called Pareto front where all the points located on it are the candidates for the optimal answer, and depending on the constraints considered by the designer, using the decision-making approaches, the best optimal answer can be selected from these candidates. In this study, the LINMAP[5] decision-making approach [47] is used for simultaneous maximization of η_{en} and η_{ex} together with minimization of LACI and LAE. The final outputs of this procedure are listed in Table 9.

The contribution of the equipment in the exergy destruction rate for all the cycles and Grassmann diagram (exergy flow) at the optimal operating conditions of the system is respectively drawn in Figs. 10 and 11. Based on Fig. 11a and b, from the total input exergy of the mover cycle (64826.2 kW), a part is utilized for power generation and heat production (20000 kW and 2384.2 kW, respectively), a part is destroyed/lost within its equipment (36920.7 kW), and the remaining part is recovered for running the bottoming sub-cycles (5521.4 kW, which is equal to $\dot{E}x_7$). From the useful recovered exergy of the mover cycle, a part is utilized for system's extra productions (409.9 kW for extra power in the RC, 145.9 kW for cold in the ERC, and 187.3 kW for hydrogen in the PEMEC), a part is spent on other systemized products or destroyed by the equipment, and finally the remaining part is discharged through the stack (2234.8 kW). This process leads to the optimal MGES exergy efficiency of 35.21%.

As can be inferred from Fig. 11, 55.4% of the input exergy is destroyed in the RGTC and HEX_1 (44.3% of this value is related to the RGTC and 11.1% for the HEX_1). The most contribution in the total exergy destruction is dedicated to the CC and it is related to the irreversible nature of the combustion reaction. After that, because of temperature difference between inlet and outlet, the HEX_1 is selected as the second source of irreversibility among all system equipment.

Fig. 12 depicts useful information about the contribution eco-environmental indices affecting the system's total cost rate at the optimal operating conditions. Analyzing the results showed that approximately half of the total cost rate, in all of the operating conditions, is related to the cost rate (46.95% of total cost rate at the optimal conditions). Another point of this figure is the significant share of the environmental penalties in the total cost rate. Although the penalty coefficient of releasing each unit of NOx is much higher than that of CO_2 and CO, the environmental penalty cost rate of NOx is negligible due to the negligible mass flow rate of NOx emission in the combustion process of the GTC. Another finding of this figure is that the RGTC, as the mover cycle, has the highest contribution in the total capital cost (48.60%: approximately half of the system's total capital cost), which is respectively followed by the ERC, PEMEC, and RC.

Fig. 13 shows the NPV during the system's life span at the optimal operating conditions. Relying on this chart, the profit reaches a positive amount approximately 5 years after the system construction, which is a reasonable payback time for such a system. As it can be inferred from the figure, the "0″ in the time ax means that one year is considered for constructing the plant and the plant operates from the year "1".

5. Conclusion, perspective, and future works

Proposing large-scale optimum MGESs based on the WHR from available conventional mono-product power plants is a substantial problem for sustainable development and grid stability. Accordingly, the aim of this study was firstly focused on the proposal and assessment of a new MGES as a district energy hub. For this, strong eco-exergy and enviro-exergy models were developed to assess the impact of design parameters on the system performance. At the second phase of the study, optimal operation of the proposed MGES was sought utilizing a powerful optimization procedure. It is worth noting that the proposed MGES comprises a RGTC, a district heating heat exchanger, a RC, an ERC, and a PEME hydrogen production unit which could simultaneously produce power, heat, cold, and hydrogen.

The outputs of the parametric analysis revealed that the design variables of the RGTC and ERC have the highest and lowest impact on the assessment criteria. So that, among all of the investigated design parameters (including the mover and bottoming cycles), the variables of PR_{COM} and PPT_{HEX_2} have the highest and lowest impact on the defined assessment criteria. Also, the criteria of η_{en} and η_{ex} were identified as the most sensitive and indifferent assessment criteria, respectively. Furthermore, after the η_{en}, the LAE was elected as the second sensitive assessment criterion.

Applying the powerful optimization procedure, the optimal operating conditions of the proposed MGES were obtained as$PR_{COM} = 12.75$,

[5] Linear Programming Technique for Multidimensional Analysis of Preference

T_{GT}=1260 K, P_{VG}=5.8 bar, PPT_{VG}=29.94 K, T_{EVA}=281 K, andPPT_{HEX_2} = 10.02 K. The corresponding system productions were included 21.42 MW of power, 26.81 MW of heat, 8.89 MW of cold, and 11.96 kg/h of hydrogen. This results in achieving the energy and exergy efficiencies of 89.75% 35.21%, respectively. In such conditions, the payback period was approximately 5 years, demonstrating the economic feasibility of the proposal.

The most important findings of the exergy, eco-exergy, and enviro-exergy analyses could also be summarized as following points: (i) Approximately half of the fuel exergy is destroyed in the RGTC and the CC is the most exergy destructive equipment. (ii) The share of fuel cost, capital cost, and environmental penalty cost are respectively 46.95%, 29.38%, and 23.67%, at the optimal conditions. (iii) Although the design variables of the bottoming cycles are not effective on the amount of pollutants (conventional environmental analysis), they have significant effect on the enviro-exergy assessment criterion (enviro-exergy analysis).

The perspective of the global energy market requires applicable energy systems based on local needs and resources. As an attractive application for the proposed MGES, in regions where the NG resources are available, in case of excess electricity production, it is possible to generate and store methane by constructing a methanation unit. This idea could be considered as an application of P2G technology and made the proposed system cleaner and more sustainable (because the flue gases of stack will be used as the required carbon source of this process).

The techno-economic and techno-environmental feasibility of using the proposed MGES was proven in this study and as some suggestions for future works on the proposed MGES, the following works are suggested: (i) Advanced exergy and eco-exergy analyses, which give a deeper understanding from technical and economic stand points. (ii) Investigating different methods for improving the techno-environmental condition of the RGTC, such as vapor injection into the CC, using biogas as the fuel, utilizing air intercooler and flue gas preheater. (iii) Evaluating the bidding strategies to manage the risk from market prices and have a maximum profit is important for having a competitive energy hub.

CRediT authorship contribution statement

Amir Ebrahimi-Moghadam: Writing – original draft, Writing – review & editing, Visualization, Methodology, Validation, Software, Investigation. **Mahmood Farzaneh-Gord:** Supervision, Project administration.

Declaration of Competing Interest

The authors declare that they have no known competing financial interests or personal relationships that could have appeared to influence the work reported in this paper.

Acknowledgement

The authors would like to thank Ferdowsi University of Mashhad for the financial support of this study.

Appendix A

The sizing of heat exchanging equipment (i.e. calculating their required heat transfer area) is the most important step for determining their cost. This section deals with presenting a procedure for reaching this objective. The required heat transfer area can be calculated through the basic heat transfer equation as follows [48].

$$A_i = \frac{\dot{Q}_i}{U_i \times (\mathrm{LMTD})_i} \tag{A1}$$

in which, the logarithmic mean temperature difference (LMTD) of the heat exchanging equipment is expressed as Eq. (A1) and U is the overall heat transfer coefficient of heat exchanger.

$$\mathrm{LMTD} = \frac{\Delta T_{\max} - \Delta T_{\min}}{\ln(\Delta T_{\max}/\Delta T_{\min})} \tag{A2}$$

The U-coefficient depends on the phase of heat exchanging flow streams. Since different streams flowing in the sub-cycles of the studied MGES have different phases, to have the same conditions, all heat exchangers are selected as shell and tube heat exchanger type. The reason for this choice is that this type of heat exchanger is applicable for different fluid phases, temperatures, and pressures. Also, for having a higher heat transfer rate, the flow

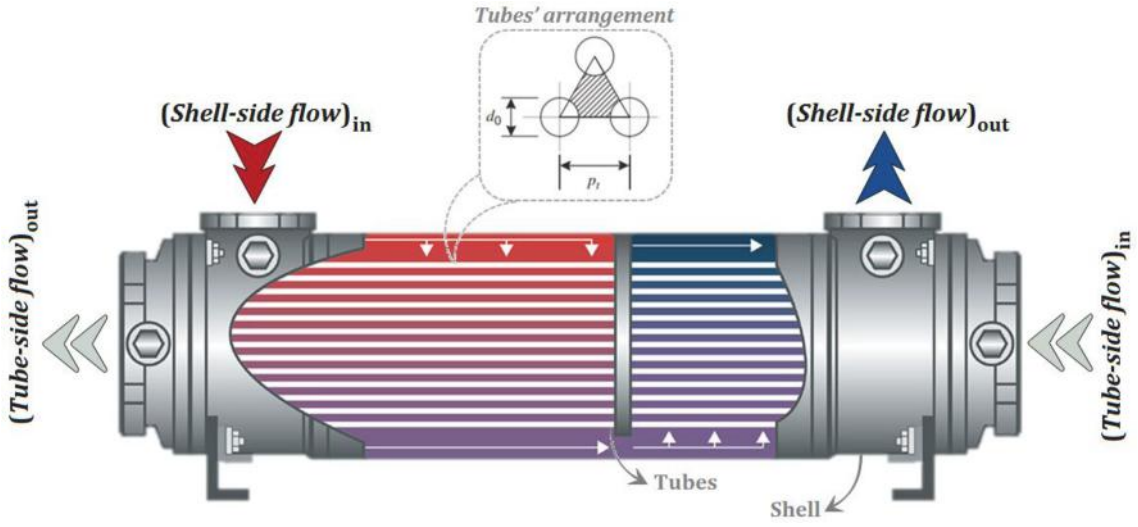

Fig. A1. Schematic diagram of the considered heat exchangers.

Table A1
Details of calculating Nusselt number for heat transfer process inside heat exchanging equipment.

Fluid stream phase	Nusselt number	Remarks
Single-phase	For tube-side stream: $Nu = 0.023Re^{0.8}Pr^{1/3}$ For shell-side stream:$Nu = 0.36Re^{0.55}Pr^{1/3}$	- The required properties of the fluid streams are determined at their corresponding mean temperature as follows: *For hot stream*: $T_{m,h} = \frac{T_{in,h} + T_{out,h}}{2}$ *For cold stream*:$T_{m,c} = \frac{T_{in,c} + T_{out,c}}{2}$
Two-phase	For condensation process: $Nu_h = 0.023Re_L^{0.8}Pr_l^{0.4}\left[(1-x)^{0.8} + 3.8\left(\frac{x^{0.76}(1-x)^{0.04}}{P^{*0.38}}\right)\right]$ For evaporation process:$Nu_c = \left(Nu_W^{2.5} + Nu_C^{2.5}\right)^{\frac{1}{2.5}}$ $Nu_W = 0.023F_W Re_l^{0.8}Pr_l^{0.4}\left(1 + \frac{1.925}{X_{tt}}\right); F_W = \begin{cases} 1; Fr_l \geq 0.25 \\ 1.23Fr_l^{0.2}; Fr_l < 0.25 \end{cases} Nu_C = 55\dot{q}^{0.67}P^{*0.12}M_{WF}^{-0.5}[-\log(P^*)]^{-0.55}\frac{d_i}{k_L}$	- This mode is used for each fluid stream in which phase change occurs (such as condensation or evaporation processes). - For condensation or evaporation processes, one fluid stream is subjected to the phase-change process (i.e. two-phase Nu correlation should be used), while the other side remains on single-phase condition (i.e. single-phase Nu correlation should be used).

streams and tubes arrangement is respectively assumed to be counter-flow and triangular. The sketch of the considered heat exchanger is schematically drawn in Fig. A1. The value of *U*-coefficient for this type of heat exchanger is expressed as Eq. (A3) [1].

$$\frac{1}{U} = \frac{1}{h_{out}} + \frac{1}{h_{in}}\frac{d_o}{d_i} + \frac{d_o}{2k}\ln\left(\frac{d_o}{d_i}\right) \tag{A3}$$

where d_i is inner diameter of tube, d_o is outer diameter of tube, k, thermal conductivity of the heat exchanger, and h is heat transfer coefficient of fluid streams. As can be inferred from this equation, the calculation of heat transfer coefficient for flow streams is the most important step for determining *U*-coefficient. These coefficients can be calculated using by the Nusselt number definition as follows:

$$h = \frac{k_{fluid} \times Nu}{D_H}, D_H = \frac{4A_c}{\mathscr{P}} \tag{A4}$$

$$D_H = \begin{cases} d_i, for\,tube-side \\ \dfrac{4\left[\frac{p_t}{2} \times 0.87p_t - \frac{1}{2}\pi\frac{d_o^2}{4}\right]}{\frac{\pi d_o}{2}} = \dfrac{1.10}{d_o}\left[p_t^2 - 0.917d_o^2\right]; p_t = 1.25d_o, for shell-side \end{cases} \tag{A5}$$

where k_{fluid}, D_H, A_c, $\mathscr{P}$, and p_t are thermal conductivity of fluid stream, hydraulic diameter, cross-sectional area, wetted perimeter by the fluid stream, and tubes pitch, respectively [49]. Also, Nu represents the Nusselt number which can be calculated using material presented in Table A1. In this table:

- The parameters Re, Pr, and Fr are the Reynolds number, Prandtl number, and Froude number, which are defined as $Re = \frac{\rho u D_H}{\mu}$, $Pr = \frac{C_p\mu}{k}$, $Fr = \frac{u}{\sqrt{gD_H}}$, respectively. Also, in the two-phase mode, the subscript "*l*" for these three parameters refers to the liquid phase (i.e. liquid fraction of the two-phase fluid). In this condition, these parameters are calculated using: $Re_l = (1-x)Re_L$, $Pr_l = (1-x)Pr_L$, and $Fr_l = (1-x)Fr_L$.

in which, the subscript "*L*" refers to situation where the working fluid is a single-phase liquid (i.e. it is assumed that all mass flowing of the working fluid is liquid). For this: $Re_L = \frac{\rho_L u_{WF} D_H}{\mu_L}$, $Pr_L = \frac{C_{PL}\mu_L}{k_L}$, and $Fr_L = \frac{u_{WF}}{\sqrt{gD_H}}$.

Also, the subscript "*V*" refers to a situation where the working fluid is completely a single-phase vapor; the subscript "WF" refers to the working fluid.

- The parameters x, $P^* = P/P_c$, $X_{tt} = \left[\left(\frac{x}{1-x}\right)^{0.9}\left(\frac{\rho_L}{\rho_V}\right)^{0.5}\left(\frac{\mu_L}{\mu_V}\right)^{0.1}\right]^{-1}$, $\dot{q}$, M, ρ, μ, and k are vapor quality, reduced pressure (in which, P_c refers to the critical pressure), Lockhart-Martinelli parameter, local heat flux, molecular weight, density, viscosity, and thermal conductivity, respectively.

References

[1] van Kleef LMT, Oyewunmi OA, Markides CN. Multi-objective thermo-economic optimization of organic Rankine cycle (ORC) power systems in waste-heat recovery applications using computer-aided molecular design techniques. Appl Energy 2019;251:112513. https://doi.org/10.1016/j.apenergy.2019.01.071.

[2] Okati V, Ebrahimi-Moghadam A, Behzadmehr A, Farzaneh-Gord M. Proposal and assessment of a novel hybrid system for water desalination using solar and geothermal energy sources. Desalination 2019;467:229–44. https://doi.org/10.1016/j.desal.2019.06.011.

[3] Water and energy, The United Nations World Water Development Report 2014 Water and Energy (Volume 1). 2014.

[4] Ebrahimi-Moghadam A, Jabari Moghadam A, Farzaneh-Gord M, Arabkoohsar A. Performance investigation of a novel hybrid system for simultaneous production of cooling, heating, and electricity. Sustain Energy Technol Assess 2021;43:100931. https://doi.org/10.1016/j.seta.2020.100931.

[5] Sadeghi S, Ghandehariun S, Rezaie B. Energy and exergy analyses of a solar-based multi-generation energy plant integrated with heat recovery and thermal energy storage systems. Appl Therm Eng 2021;188:116629. https://doi.org/10.1016/j.applthermaleng.2021.116629.

[6] Karapekmez A, Dincer I. Development of a multigenerational energy system for clean hydrogen generation. J Clean Prod 2021;299:126909. https://doi.org/10.1016/j.jclepro.2021.126909.

[7] Li Y, Liu Y, Zhang G, Yang Y. Thermodynamic analysis of a novel combined cooling and power system utilizing liquefied natural gas (LNG) cryogenic energy and low-temperature waste heat. Energy 2020;199:117479. https://doi.org/10.1016/j.energy.2020.117479.

[8] Bloess A. Modeling of combined heat and power generation in the context of increasing renewable energy penetration. Appl Energy 2020;267:114727. https://doi.org/10.1016/j.apenergy.2020.114727.

[9] Zhang H, Wang L, Lin X, Chen H. Combined cooling, heating, and power generation performance of pumped thermal electricity storage system based on Brayton cycle. Appl Energy 2020;278:115607. https://doi.org/10.1016/j.apenergy.2020.115607.

[10] Ding P, Zhang Ke, Yuan Z, Wang Z, Li D, Chen T, et al. Multi-objective optimization and exergoeconomic analysis of geothermal-based electricity and cooling system using zeotropic mixtures as the working fluid. J Clean Prod 2021;294:126237. https://doi.org/10.1016/j.jclepro.2021.126237.

[11] Cao Y, Mihardjo LWW, Dahari M, Tlili I. Waste heat from a biomass fueled gas turbine for power generation via an ORC or compressor inlet cooling via an absorption refrigeration cycle: A thermoeconomic comparison. Appl Therm Eng 2021;182:116117. https://doi.org/10.1016/j.applthermaleng.2020.116117.

[12] Chitgar N, Moghimi M. Design and evaluation of a novel multi-generation system based on SOFC-GT for electricity, fresh water and hydrogen production. Energy 2020;197:117162. https://doi.org/10.1016/j.energy.2020.117162.

[13] Zoghi M, Habibi H, Yousefi Choubari A, Ehyaei MA. Exergoeconomic and environmental analyses of a novel multi-generation system including five subsystems for efficient waste heat recovery of a regenerative gas turbine cycle with hybridization of solar power tower and biomass gasifier. Energy Convers Manage 2021;228:113702. https://doi.org/10.1016/j.enconman.2020.113702.

[14] Park C, Jung Y, Lim K, Kim B, Kang Y, Ju H. Analysis of a phosphoric acid fuel cell-based multi-energy hub system for heat, power, and hydrogen generation. Appl Therm Eng 2021;189:116715. https://doi.org/10.1016/j.applthermaleng.2021.116715.

[15] Safder U, Nguyen H-T, Ifaei P, Yoo C. Energetic, economic, exergetic, and exergorisk (4E) analyses of a novel multi-generation energy system assisted with bagasse-biomass gasifier and multi-effect desalination unit. Energy 2021;219:119638. https://doi.org/10.1016/j.energy.2020.119638.

[16] Nazari N, Porkhial S. Multi-objective optimization and exergo-economic assessment of a solar-biomass multi-generation system based on externally-fired gas turbine, steam and organic Rankine cycle, absorption chiller and multi-effect desalination. Appl Therm Eng 2020;179:115521. https://doi.org/10.1016/j.applthermaleng.2020.115521.

[17] Azariyan H, Vajdi M, Rostamnejad TH. Assessment of a high-performance geothermal-based multigeneration system for production of power, cooling, and hydrogen: Thermodynamic and exergoeconomic evaluation. Energy Convers Manag 2021;236:113970. https://doi.org/10.1016/j.enconman.2021.113970.

[18] Peláez-Peláez S, Colmenar-Santos A, Pérez-Molina C, Rosales A-E, Rosales-Asensio E. Techno-economic analysis of a heat and power combination system based on hybrid photovoltaic-fuel cell systems using hydrogen as an energy vector. Energy 2021;224:120110. https://doi.org/10.1016/j.energy.2021.120110.

[19] Ebrahimi-Moghadam A, Farzaneh-Gord M, Jabari Moghadam A, Abu-Hamdeh NH, Lasemi MA, Arabkoohsar A, et al. Design and multi-criteria optimisation of a trigeneration district energy system based on gas turbine, Kalina, and ejector cycles: Exergoeconomic and exergoenvironmental evaluation. Energy Convers Manage 2021;227:113581. https://doi.org/10.1016/j.enconman.2020.113581.

[20] Di Marcoberardino G, Chiarabaglio L, Manzolini G, Campanari S. A Techno-economic comparison of micro-cogeneration systems based on polymer electrolyte membrane fuel cell for residential applications. Appl Energy 2019;239:692–705. https://doi.org/10.1016/j.apenergy.2019.01.171.

[21] Lümmen N, Karouach A, Tveitan S. Thermo-economic study of waste heat recovery from condensing steam for hydrogen production by PEM electrolysis. Energy Convers Manag 2019;185:21–34. https://doi.org/10.1016/j.enconman.2019.01.095.

[22] Alirahmi SM, Razmi AR, Arabkoohsar A. Comprehensive assessment and multi-objective optimization of a green concept based on a combination of hydrogen and compressed air energy storage (CAES) systems. Renew Sustain Energy Rev 2021;142:110850. https://doi.org/10.1016/j.rser.2021.110850.

[23] Ahmadi A, Jamali DH, Ehyaei MA, Assad MEH. Energy, exergy, economic and exergoenvironmental analyses of gas and air bottoming cycles for production of electricity and hydrogen with gas reformer. J Clean Prod 2020;259:120915. https://doi.org/10.1016/j.jclepro.2020.120915.

[24] Li Z, Khanmohammadi S, Khanmohammadi S, Al-Rashed AAAA, Ahmadi P, Afrand M. 3-E analysis and optimization of an organic Rankine flash cycle integrated with a PEM fuel cell and geothermal energy. Int J Hydrogen Energy 2020;45:2168–85. https://doi.org/10.1016/j.ijhydene.2019.09.233.

[25] Datas A, Ramos A, del Cañizo C. Techno-economic analysis of solar PV power-to-heat-to-power storage and trigeneration in the residential sector. Appl Energy 2019;256:113935. https://doi.org/10.1016/j.apenergy.2019.113935.

[26] Moharamian A, Soltani S, Rosen MA, Mahmoudi SMS, Morosuk T. Exergoeconomic analysis of natural gas fired and biomass post-fired combined cycle with hydrogen injection into the combustion chamber. J Clean Prod 2018;180:450–65. https://doi.org/10.1016/j.jclepro.2018.01.156.

[27] Deymi-Dashtebayaz M, Ebrahimi-Moghadam A, Pishbin SI, Pourramezan M. Investigating the effect of hydrogen injection on natural gas thermo-physical properties with various compositions. Energy 2019;167:235–45. https://doi.org/10.1016/j.energy.2018.10.186.

[28] Emadi MA, Chitgar N, Oyewunmi OA, Markides CN. Working-fluid selection and thermoeconomic optimisation of a combined cycle cogeneration dual-loop organic Rankine cycle (ORC) system for solid oxide fuel cell (SOFC) waste-heat recovery. Appl Energy 2020;261:114384. https://doi.org/10.1016/j.apenergy.2019.114384.

[29] Ebrahimi-Moghadam A, Deymi-Dashtebayaz M, Jafari H, Niazmand A. Energetic, exergetic, environmental and economic assessment of a novel control system for indirect heaters in natural gas city gate stations. J Therm Anal Calorim 2020;141(6):2573–88. https://doi.org/10.1007/s10973-020-09413-4.

[30] Alirahmi SM, Bashiri Mousavi S, Razmi AR, Ahmadi P. A comprehensive techno-economic analysis and multi-criteria optimization of a compressed air energy storage (CAES) hybridized with solar and desalination units. Energy Convers Manage 2021;236:114053. https://doi.org/10.1016/j.enconman.2021.114053.

[31] Ebadollahi M, Rostamzadeh H, Ghaebi H, Amidpour M. Exergoeconomic analysis and optimization of innovative cascade bi-evaporator electricity/cooling cycles with two adjustable cooling temperatures. Appl Therm Eng 2019;152:890–906. https://doi.org/10.1016/j.applthermaleng.2019.02.110.

[32] Cao Y, Dhahad HA, Togun H, Anqi AE, Farouk N, Farhang B. A novel hybrid biomass-solar driven triple combined power cycle integrated with hydrogen production: Multi-objective optimization based on power cost and CO2 emission. Energy Convers Manage 2021;234:113910. https://doi.org/10.1016/j.enconman.2021.113910.

[33] Wu Z, Zhu P, Yao J, Zhang S, Ren J, Yang F, et al. Combined biomass gasification, SOFC, IC engine, and waste heat recovery system for power and heat generation: energy, exergy, exergoeconomic, environmental (4E) evaluations. Appl Energy 2020;279:115794. https://doi.org/10.1016/j.apenergy.2020.115794.

[34] Al-Rashed AAAA, Afrand M. Multi-criteria exergoeconomic optimization for a combined gas turbine-supercritical CO2 plant with compressor intake cooling fueled by biogas from anaerobic digestion. Energy 2021;223:119997. https://doi.org/10.1016/j.energy.2021.119997.

[35] Bo Z, Mihardjo LWW, Dahari M, Abo-Khalil AG, Al-Qawasmi A-R, Mohamed AM, et al. Thermodynamic and exergoeconomic analyses and optimization of an auxiliary tri-generation system for a ship utilizing exhaust gases from its engine. J Clean Prod 2021;287:125012. https://doi.org/10.1016/j.jclepro.2020.125012.

[36] Moghimi M, Emadi M, Ahmadi P, Moghadasi H. 4E analysis and multi-objective optimization of a CCHP cycle based on gas turbine and ejector refrigeration. Appl Therm Eng 2018;141:516–30. https://doi.org/10.1016/j.applthermaleng.2018.05.075.

[37] Ebrahimi-Moghadam A, Moghadam AJ, Farzaneh-Gord M, Aliakbari K. Proposal and assessment of a novel combined heat and power system: energy, exergy, environmental and economic analysis. Energy Convers Manage 2020;204:112307. https://doi.org/10.1016/j.enconman.2019.112307.

[38] Boyaghchi FA, Chavoshi M, Sabeti V. Multi-generation system incorporated with PEM electrolyzer and dual ORC based on biomass gasification waste heat recovery: Exergetic, economic and environmental impact optimizations. Energy 2018;145:38–51. https://doi.org/10.1016/j.energy.2017.12.118.

[39] Ebrahimi-Moghadam A, Moghadam AJ, Farzaneh-Gord M. Comprehensive techno-economic and environmental sensitivity analysis and multi-objective optimization of a novel heat and power system for natural gas city gate stations. J Clean Prod 2020;262:121261. https://doi.org/10.1016/j.jclepro.2020.121261.

[40] Shokouhi Tabrizi AH, Niazmand H, Farzaneh-Gord M, Ebrahimi-Moghadam A. Energy, exergy and economic analysis of utilizing the supercritical CO2 recompression Brayton cycle integrated with solar energy in natural gas city gate station. J Therm Anal Calorim 2021;145(3):973–91. https://doi.org/10.1007/s10973-020-10241-9.

[41] Nami H, Anvari-Moghaddam A. Geothermal driven micro-CCHP for domestic application – exergy, economic and sustainability analysis. Energy 2020;207:118195. https://doi.org/10.1016/j.energy.2020.118195.

[42] Dincer I, Rosen MA, Ahmadi P. Modeling and optimization of multigeneration energy systems. Optim. Energy Syst. 2017:398–446. https://doi.org/10.1002/9781118894484.ch11.

[43] Nemati A, Nami H, Ranjbar F, Yari M. A comparative thermodynamic analysis of ORC and Kalina cycles for waste heat recovery: a case study for CGAM cogeneration system. Case Stud Therm Eng 2017;9:1–13. https://doi.org/10.1016/j.csite.2016.11.003.

[44] Yapıcı R, Ersoy HK, Aktoprakoğlu A, Halkacı HS, Yiğit O. Experimental determination of the optimum performance of ejector refrigeration system depending on ejector area ratio. Int J Refrig 2008;31:1183–9. https://doi.org/10.1016/j.ijrefrig.2008.02.010.
[45] Ioroi T, Yasuda K, Siroma Z, Fujiwara N, Miyazaki Y. Thin film electrocatalyst layer for unitized regenerative polymer electrolyte fuel cells. J Power Sources 2002;112:583–7. https://doi.org/10.1016/S0378-7753(02)00466-4.
[46] Farzaneh-Gord M, Mohseni-Gharyehsafa B, Ebrahimi-Moghadam A, Jabari-Moghadam A, Toikka A, Zvereva I. Precise calculation of natural gas sound speed using neural networks: An application in flow meter calibration. Flow Meas Instrum 2018;64:90–103. https://doi.org/10.1016/j.flowmeasinst.2018.10.013.
[47] Ebrahimi-Moghadam A, Kowsari S, Farhadi F, Deymi-Dashtebayaz M. Thermohydraulic sensitivity analysis and multi-objective optimization of Fe3O4/H2O nanofluid flow inside U-bend heat exchangers with longitudinal strip inserts. Appl Therm Eng 2020;164:114518. https://doi.org/10.1016/j.applthermaleng.2019.114518.
[48] Han Z, Li P, Han Xu, Mei Z, Wang Z. Thermo-economic performance analysis of a regenerative superheating organic Rankine cycle for waste heat recovery. Energies 2017;10(10):1593. https://doi.org/10.3390/en10101593.
[49] Towler G, Sinnott R. Chemical Engineering Design. 2nd ed. Elsevier; 2012.
[50] Wang A, Wang S, Ebrahimi-Moghadam A, Farzaneh-Gord M, Moghadam AJ. Techno-economic and techno-environmental assessment and multi-objective optimization of a new CCHP system based on waste heat recovery from regenerative Brayton cycle. Energy 2021:122521. https://doi.org/10.1016/j.energy.2021.122521.